XV. NEUROLOGY*

L. Stark
Anne Crider
G. Cook
J. F. Dickson III
J. Grossman
H. Horibe
M. Lorber
D. Martin
G. A. Masek
J. A. Michael
D. Miller
H. Miyahara
A. Natapoff
J. Negrete
O. Sanchez-Felipe
A. A. Sandberg
J. I. Simpson
S. F. Stanten
H. H. Sun
G. Theodoridis
G. H. Whipple
Guillermina N. Yankelevich
B. L. Zuber

A. COMPUTER PATTERN-RECOGNITION TECHNIQUES: REMOTE ON-LINE, REAL-TIME COMPUTER SYSTEM FOR DIAGNOSIS OF CLINICAL ELECTROCARDIOGRAMS

Recent advances in digital computation techniques have made it possible to approach the problem of automatic diagnosis of the clinical electrocardiogram (EKG) with confidence that a solution will be found. Our research has been mainly concerned with the application of adaptive matched-filter pattern-recognition techniques to EKG diagnosis.

In previous publications we have (a) shown that the multiple adaptive matched-filter technique was an efficient means for sorting a number of EKG tracings into groups resembling each other; (b) described our experience with the application of this technique to real EKG on a digital computer for the purpose of recognizing and classifying data resulting from automatic time normalization and synchronization, and observed the accuracy with which the QRS complex patterns are sorted or recognized when compared with precisely known diagnosed complexes; and (c) compared human and machine classification of known reference complexes into a predetermined number of groups.

Recently, a series of typical filter patterns for the P, QRS, and ST-T segments of the EKG has been developed; a diagnostic program for rhythm analysis has been prepared; interpretation and diagnostic matrices have been devised which incorporate pattern recognition, rhythm, and extracted parameter data with some stratifying clinical information for the determination of a final EKG diagnosis; the loop of the diagnostic system has been closed by the frequency-modulated transmission of EKG data by telephone lines from the Electrocardiography Laboratory of the Massachusetts Memorial Hospital to a G.E. 225 digital computer at M.I.T. and the subsequent return of a diagnosis to the hospital laboratory for teletype display; and an executive monitoring routine has been incorporated into the program which allows remote teletype control of the diagnostic system by a technician at the hospital laboratory. The introduction of these features has resulted in a remote on-line, real-time digital-computer system for EKG

*Major support for this research is provided by the U.S. Public Health Service (B-3055-4, B-3090-4, MH-06175-02), the U.S. Navy (Office of Naval Research (Nonr-1841(70)), the U.S. Air Force (AF49(638)-1313), administered by the Electronic Systems Laboratory, M.I.T.

diagnosis. This report briefly describes the system configuration and its function.

The interconnections of the remote diagnostic system are shown in Fig. XV-1. In the Electrocardiography Laboratory a lead system selector accommodates the standard leads and the SVEC III, Frank, and Grishman vectorcardiographic lead systems, including a calibration circuit for 0.1, 0.5, and 1.0, and 2.0 mv. Differential amplifiers are used for the amplification of the EKG, and the frequency-response passband is set between 0.2 cps and 250 cps. Operational amplifier units are now being used as a buffer to add DC bias voltage and to adjust amplification. Teletype communication by telephone line from the hospital laboratory to the computer at M.I.T. allows a hospital technician to maintain executive control of the diagnostic system at M.I.T., and to monitor the transmission of the patient's identification number, pertinent clinical information, and the electrocardiographic signals to the computer. The EKG data are also transmitted by a frequency-modulated system by telephone line. At M.I.T. the transmitted signal is demodulated and enters the G.E. 225 computer through its analog-to-digital converter. The EKG signal is then processed and analyzed. The resultant diagnosis is automatically returned by telephone line to the hospital where it is displayed as a teletype print-out.

Figure XV-2 is a block diagram of the operational sequences of the diagnostic program. Initially, the executive monitor, which is used by the hospital technician for remote control of the sequence of operations, is placed in the computer. The diagnostic process is instituted by the hospital technician with the transmission of the patient's data and the electrocardiographic tracings to the computer at M.I.T.

The EKG signals originating in the hospital are often obscured by noise, and preprocessing is necessary to facilitate rhythm interpretation, pattern recognition, and parameter extraction. In the preprocessing section the signals are first smoothed by a least-squares parabolic method. The complexes are then averaged to provide a further smoothing effect. Averaging to remove the low-frequency nonsynchronous noise is particularly effective here.

In the rhythm section, the atrial rate is determined by an averaging routine in which template subtraction eliminates the QRS-T portion of a number of successive beats and allows for a P-P interval determination. The ventricular rate is determined by calculation of the R-R interval on the first derivation of the EKG tracing. The presence or absence of atrial or ventricular premature beats is assessed by a floating average technique. These combined data are analyzed by a rhythm tree, which yields approximately 20 mutually exclusive, tentative, rhythm interpretations. In the morphological identification section of the program, the current filters are analyzing the X-lead of Frank's orthogonal lead system. The preprocessed signal is submitted to point recognition and to time and amplitude normalization. The P, QRS, and ST-T segments are then introduced into the adaptive matched-filter pattern-recognition programs, which provide tentative pattern-recognition interpretations. After point recognition, the

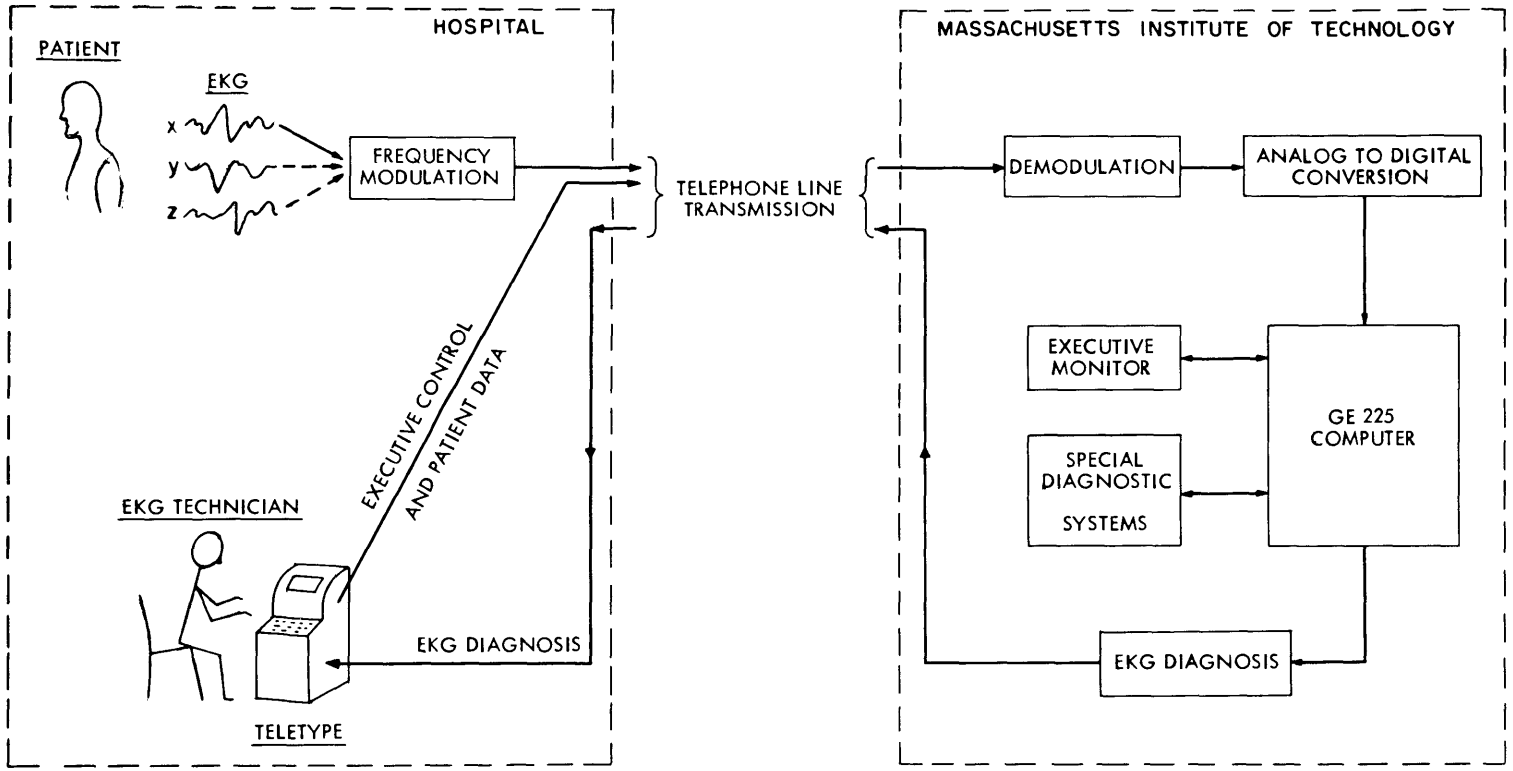

Fig. XV-1. Remote on-line, real-time EKG diagnostic system.

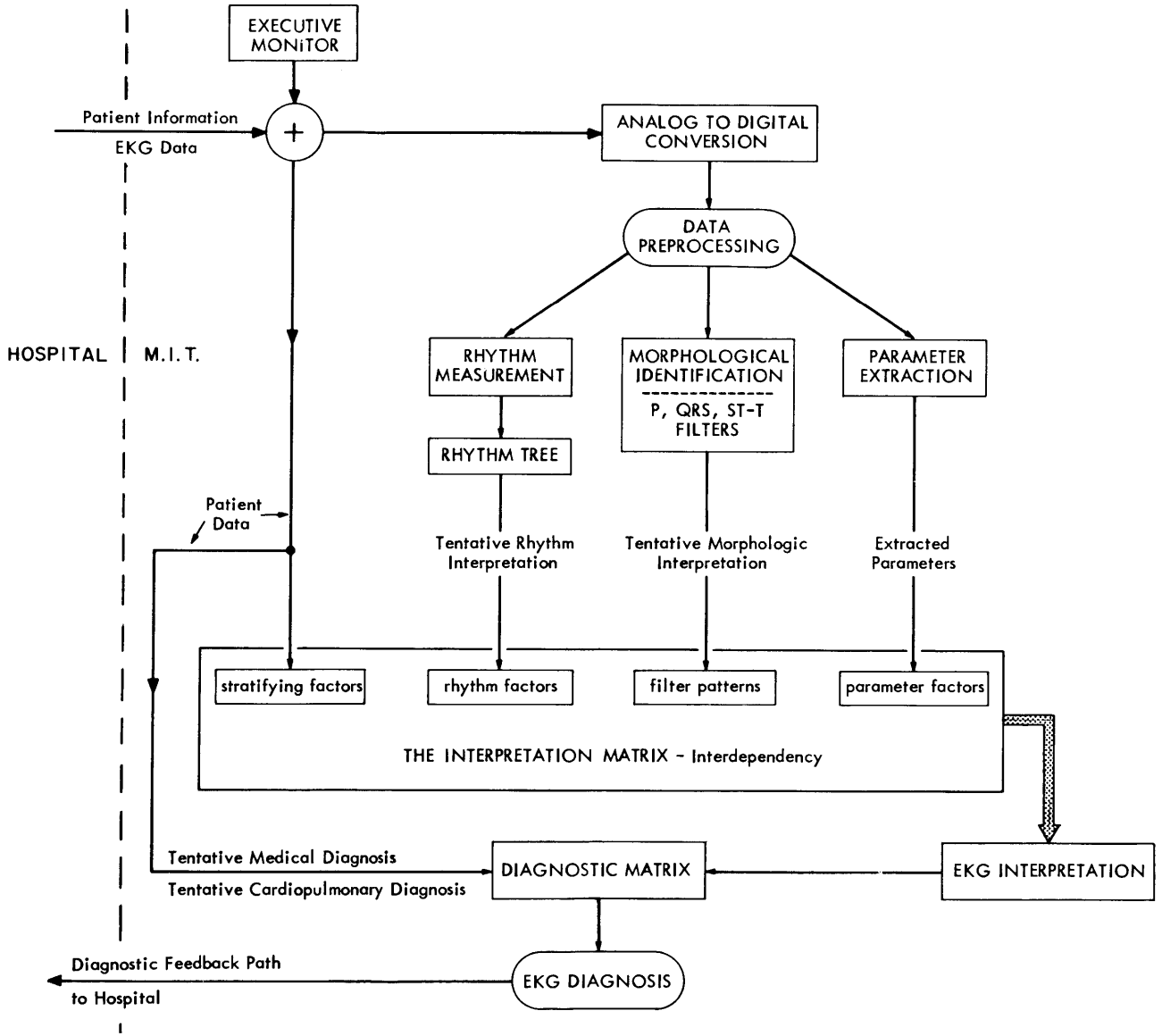

Fig. XV-2. Sequence of the EKG diagnostic system.

parameter-extracting portion of the program makes pertinent determinations that relate to amplitude (as amplitude of the QRS complex) and interval (as the Q-T interval).

The interpretation matrix is that section of the diagnostic sequence in which the independent determinations of rhythm, pattern recognition, and extracted parameters are allowed to interrelate. Stratifying factors (such as age, sex, ponderal index, drugs, etc.) are also admitted to the diagnostic sequence at this point in the program. The matrix itself is a Chapman additive pattern-recognition matrix in which the ratio of the maximum to the mean element value is proportional to the number of the matrix inputs. Fixed weightings are assigned for the various diagnostic criteria, and the matrix yields

```
NAME      ALICE LEARY
HOSP. IDENT. NO. 127645

----------------------------------------


1.   TENTATIVE INTERPRETATION

       A. RHYTHM ANALYSIS
            VENTRICULAR PREMATURE BEAT WITH COMPENSATORY PAUSE
            1 IN 16

       B. AMPLITUDES AND TIME INTERVALS
            HEART RATE 82
            AMPLITUDES  MV
                ST SEGMENT 0.03  0.04  0.08
                P  0.12  Q -0.06  R 1.34  S -0.37  T 0.38
            DURATIONS  SEC
               P  0.11  QRS 0.11  PQ 0.16  QT  0.38

       C. PATTERN INTERPRETATION WITH CORRELATION COEFFICIENT
            P PULMONALE 0.36
            INCOMPLETE RIGHT BUNDLE  BRANCH BLOCK 0.84
            NORMAL T WAVE 0.63


11.  ELECTROCARDIOGRAPHIC INTERPRETATION

        NORMAL HEART RATE  82 PER MIN.
        VENTRICULAR PREMATURE BEAT WITH COMPENSATORY PAUSE 1 IN 16
        INCOMPLETE RIGHT BUNDLE BRANCH BLOCK


111. ELECTROCARDIOGRAPHIC DIAGNOSIS
        VENTRICULAR PREMATURE BEATS WITH COMPENSATORY PAUSE 1 IN 16
        UNCOMPLICATED INCOMPLETE RIGHT BUNDLE BRANCH BLOCK
```

Fig. XV-3. Teletyped diagnostic print-out.

approximately 25 EKG interpretations. These interpretations can then be incorporated in a second matrix with the tentative clinical and cardiopulmonary diagnoses (when they are available) for the production of a final EKG diagnosis. This diagnosis is returned for display by teletype in the hospital laboratory.

There are 8192 memory locations in the computer. This is not enough to store the minimum required length of the EKG signal and the entire program at the same time. Operationally, therefore, the diagnostic system consists of a sequence of five programs that are called into memory by the executive monitoring program. This subdivision of system programming is necessary not only because of the limited memory space but also partly because compiler programming is used in the majority of the sequences.

Diagnostic runs are made twice daily. The operation time for each case is approximately 4 minutes, with half of the time consumed by teletyping and tape handling and the rest by real-time computation.

A typical teletype from this diagnostic system is shown in Fig. XV-3. In addition to the patient's identification factors, the output consists of three parts: (i) the tentative, isolated interpretations relating to rhythm, morphological interpretation, and extracted parameters; (ii) the EKG interpretation; and (iii) the final EKG diagnosis. The results of the analysis are presented in this sequential form to provide a clear picture of the sectional contributions to the final diagnosis and to allow for on-line, real-time computer diagnosis with interaction between cardiologist and computer at various levels in the diagnostic process during those periods when an attempt is being made to increase the diagnostic accuracy of the system. These interacting runs are adapted to the variety of available clinical material. Although the remote diagnostic studies thus far have been conducted from the Electrocardiography Laboratory at the hospital, a portable cart containing an electrocardiograph, a teletype, and data-transmission equipment is being readied to provide bedside diagnostic service throughout the hospital.

Our present efforts to extend the diagnostic capabilities of the system are particularly concerned with increased fidelity of the adaptive matched filters, development of three-dimensional pattern analysis, analysis of parallel diagnostic efforts by electrocardiographer and computer, and the study of the advisability and possibility of the introduction of major treelike branching decisions early in the diagnostic process.

J. F. Dickson III, G. H. Whipple, H. Horibe, J. Grossman, L. Stark

B. SAMPLED-DATA CHARACTERISTICS OF HAND-TRACKING AND EYE-TRACKING SYSTEMS

Figure XV-4 shows an experimental apparatus that is being used to study human tracking responses to constant-velocity targets. The subject is seated 18 inches in front of a translucent plastic screen. Resting his head on a stabilizing device, the subject

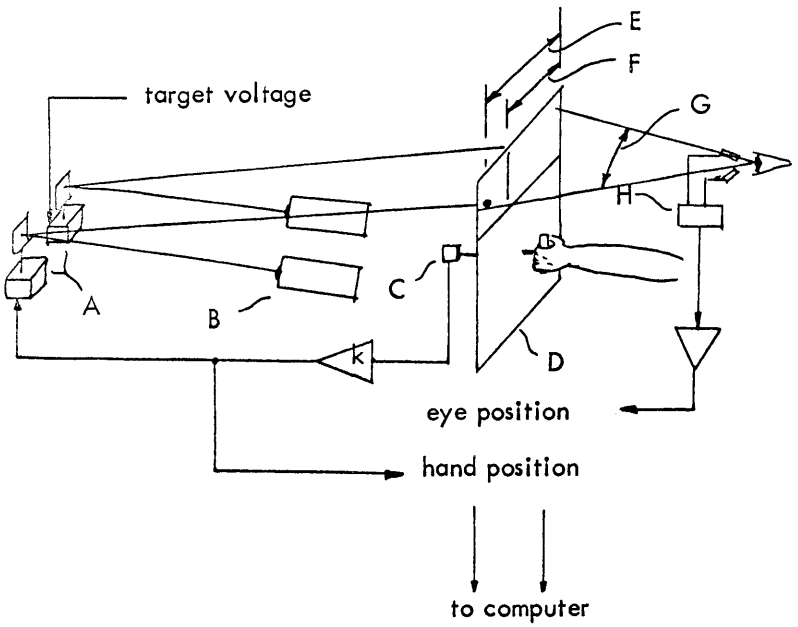

A	mirror galvanometers	E	hand deflection
B	light sources (slit and spot)	F	target deflection
C	angular readout potentiometer	G	maximum eye angle range
D	projection screen	H	eye movement detector

Fig. XV-4. Diagram of experimental apparatus.

wears a photoelectric eye-movement detector.[1] Below the screen is a handle that can rotate freely and whose angle is measured by a low-torque potentiometer.

A blue line and a white spot of light are cast upon the screen from behind. Two independent galvanometer-driven mirrors control the respective deflections of the two images. The galvanometer inputs are hand angle (multiplied by a variable gain K), and target signal. Thus, as the subject rotates the handle, the white spot moves horizontally in proportion to the hand angle. The subject attempts to keep the spot coincident with the generator-controlled line.

The use of photoconductive diodes in the eye-movement detector yields exceptionally clean data. Figure XV-5 shows a calibration recording wherein the subject was told to move the white spot by rotating the handle and to follow the white spot visually. This method of calibration uniquely defines the static and dynamic calibration constants for the Sanborn recorder.

For this series of experiments the G. E. 225 computer served as a ramp train generator, capable of generating ramps with random or periodic velocities. It is instructive to observe some typical tracking responses to random and periodic ramps.

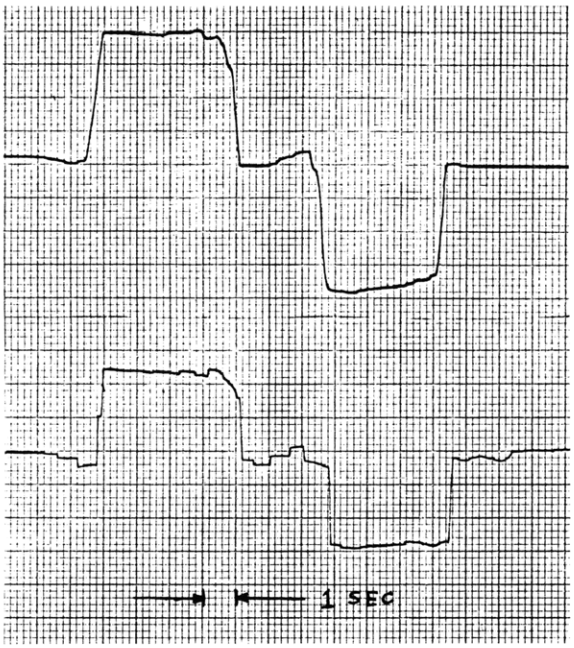

Fig. XV-5.

Calibration recording: Upper trace, hand. Lower trace, eye. Deflection: left 6 inches, right 6 inches.

Figure XV-6 is a recording of random ramp responses. The dissimilarity in the nature of the eye-tracking and hand-tracking systems is evident. Young and Stark[2] have suggested that the eye-tracking system operating on unpredictable inputs is

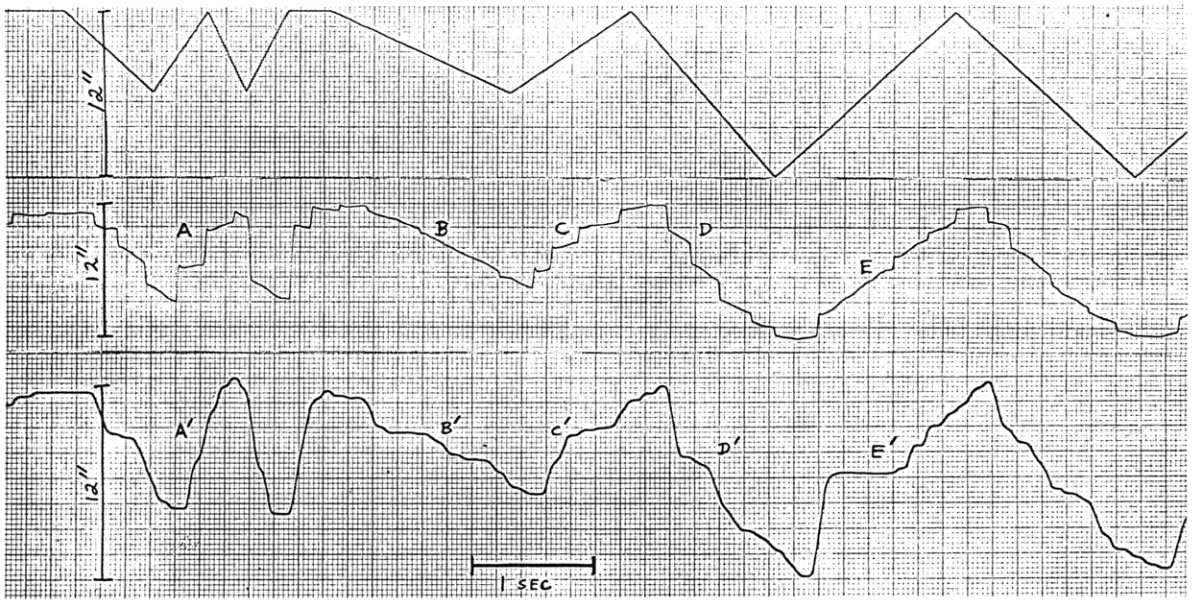

Fig. XV-6. Observed responses to random input ramp. Upper trace, target position (12-inch deflection). Middle trace, eye position. Lower trace, hand position.

characterized by a sampled-position servomechanism that controls saccadic responses, and by a sampled-velocity servomechanism that controls constant-velocity responses. The system is expected to switch between its two modes when the input velocity saturates the velocity pursuit system (25° per second), or when a positional error is accumulated. The over-all eye-movement system cannot issue a corrective command between clock-controlled sample periods.

In Fig. XV-6, waveform A demonstrates the velocity-system saturation yielding the positional rather than constant-velocity segments. Contrast this with waveforms C and D wherein constant-velocity segments are observed, and the accumulation of position errors causes position saccades. Dissimilarly, waveform B demonstrates segments of constant correct velocity with no corrective saccades. The eye and orbit are characterized by very fast second-order dynamics that can be neglected in comparison with the sampling dynamics.

The lower trace in Fig. XV-6 demonstrates the typical intermittent responses that characterize hand response. Naves[3,4] has suggested that a possible explanation for such intermittency is the existence of a sampler in the hand-tracking system. The mechanical time constants of the arm, however, are such as to obscure clear observation of the sampling dynamics.

A further dissimilarity between the hand- and eye-tracking systems is illustrated

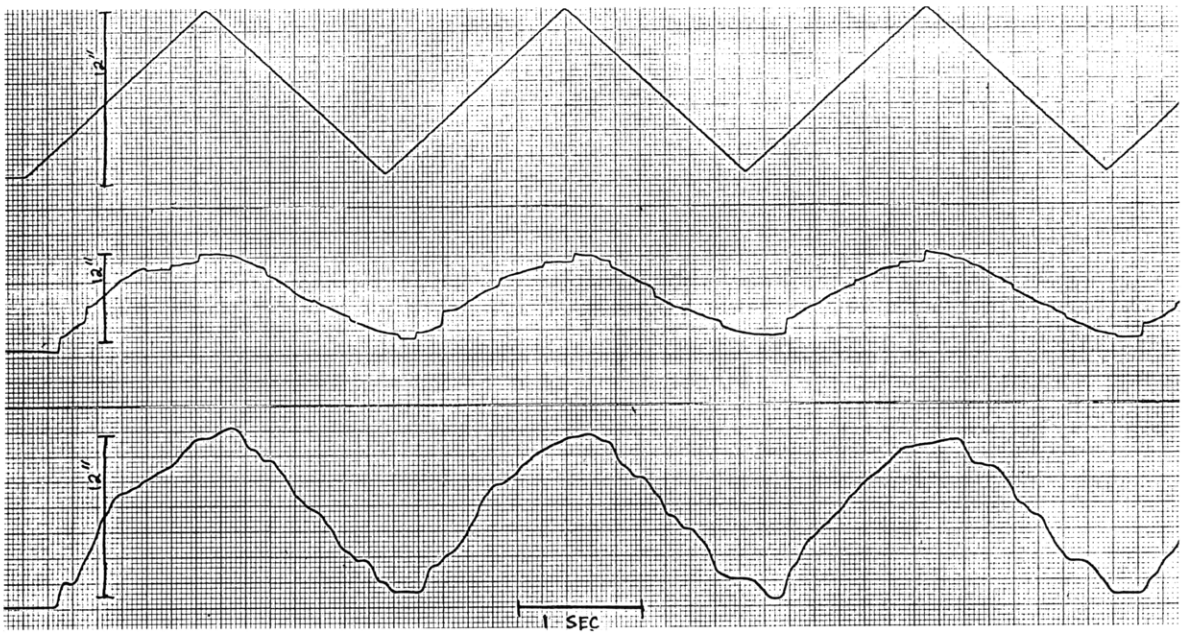

Fig. XV-7. Observed responses to periodic predictable input ramp. Upper trace, target position. Middle trace, eye position. Lower trace, hand position.

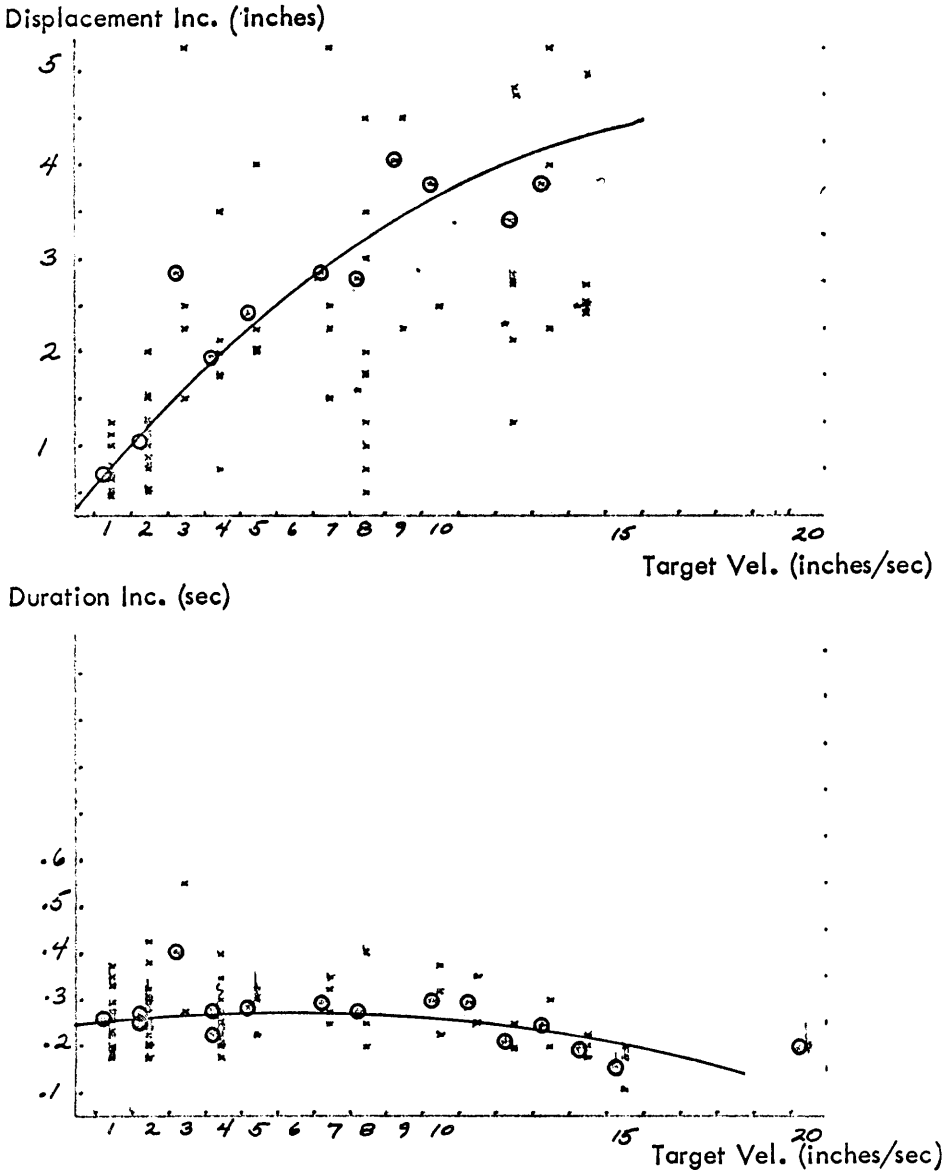

Fig. XV-8. Plots showing quasi-linear relation between displacements and target velocity, and quasi-constant relation between duration increments and target velocity.

in Fig. XV-7, which shows the responses to a periodic ramp train. The three target cycles shown are the first three in a run of twenty. Observe that in the third cycle, the eye is predicting the waveform accurately to the extent that few corrective saccades are present. Young demonstrated that for predictable inputs the eye-movement system was best characterized by a fourth-order continuous model. The presence of some clocked corrective saccades, minor but present, does not constitute, for this case, a contradiction of Young's model, for two reasons. First, it can be shown that prediction of a periodic waveform with a long period is difficult; therefore, the eye may not be in a steady state of prediction. Second, Young's model is based essentially on compensatory tracking, for in his work only one display (the target) was visible. In our case, two images are present. It is possible that the intermittency of the hand position might trigger eye saccades, even though the eye was predicting target position. Notice that the over-all nature of the hand response does not change drastically as would be expected with adaptation to the periodic input. Qualitatively, few intermittent inflections appear during adaptation and the over-all waveform is somewhat smoother, but the change is small. This suggests that the sampler in the hand-tracking system is not under direct control of the central nervous system (CNS), but is located in the output elements.

One may show that indeed the intermittency is explained by the presence of a sampler by plotting the step magnitude (displacement increment) and step duration (duration increment) against target velocity. Figure XV-8 demonstrates such a plot. The almost linear relation between duration increment and target velocity suggests the existence of a sampler. That the sampler does not operate at a constant interval, however, can be seen by the plot of duration increment against target velocity.

By using the multiplicative constant, K (between the handle and galvanometer) as a parameter, we have undertaken a series of experiments[5] to explain the nature of the variable sampler, and to verify its location in the peripheral transducers rather than in the CNS.

Preliminary evidence shows that the hand-tracking system may be characterized by a sampled model, which is quite dissimilar to the sampled eye-tracking model. The relatively small inertial and viscous loads seen by the eye muscles allow observation of the sampling dynamics more readily than in the hand-tracking system.

G. A. Masek, L. Stark

References

1. G. P. Nelson and L. Stark, Phototube glasses for measuring eye movement, Quarterly Progress Report No. 67, Research Laboratory of Electronics, M.I.T., October 15, 1962, pp. 214-216.

2. L. R. Young and L. Stark, A sampled-data model for eye-tracking movements, Quarterly Progress Report No. 66, Research Laboratory of Electronics, M.I.T., July 15, 1962, pp. 379-384.

3. F. Naves, Sampling of Quantization in the Human Tracking System, S. B. Thesis, Department of Electrical Engineering, M. I. T., January 1963.

4. F. Naves and L. Stark, Experiments on discrete control of hand movement, Quarterly Progress Report No. 69, Research Laboratory of Electronics, M. I. T., April 15, 1963, pp. 256-258.

5. G. A. Masek, The Sampling Process in Human Visuo-Motor Tracking, S. M. Thesis, Department of Electrical Engineering, M. I. T., September 1964.

C. MARKOV MODELING TECHNIQUE FOR PREDICTABLE VISUO-MOTOR TRACKING

Analysis of the human's responses while tracking predictable waveforms is complex because of over-all qualitative response changes as the subject adapts to the predictable waveform. Once adapted to such an input, the human uses higher cortical centers to preprogram his responses. A general model capable of quantitative comparison of two or more tracking systems is desired.

Billheimer[1] proposed a probabilistic method in the form of a partitioned Markov model that can account for the memory dependence of the learning of a periodic predictable waveform. Using the techniques developed by Billheimer, we have written a program for the G. E. 225 computer to test the validity of the partitioned Markov model in a human tracking experiment. It is instructive to describe the characteristics of the theoretical model, as well as its computer implementation.

1. Markov Model

A simple Markov chain[2] is history-independent. We seek a method by which we may build memory dependence into the system, yet retain the relative simplicity of the original chain. If the probability that a system in state i will make a transition to state j is dependent upon h, which is the state of the system before state i, we may expand states h, i, and j to a new set of states such that the dependent probability no longer exists, but is embodied in the expanded states (Fig. XV-9).

The prior state-dependent transition probability is a weighted sum of the expanded state transition probabilities.[1,2] By suitably expanding states in a particular part of a transition diagram one can, in essence, build in memory dependence, while retaining the simple Markov chain configuration. Extending this method, we can account for higher order memory dependence by further expanding the states in the original model.

Accurate prediction of mean passage time from one point in the transition diagram to some other point of significance and inaccurately large predictions of the variance passage time are general characteristics of simple Markov models. If we define accuracy criteria of the model in terms of correct mean and variance passage time predictions, then we may introduce dummy or holding states in series with existing states. Billheimer

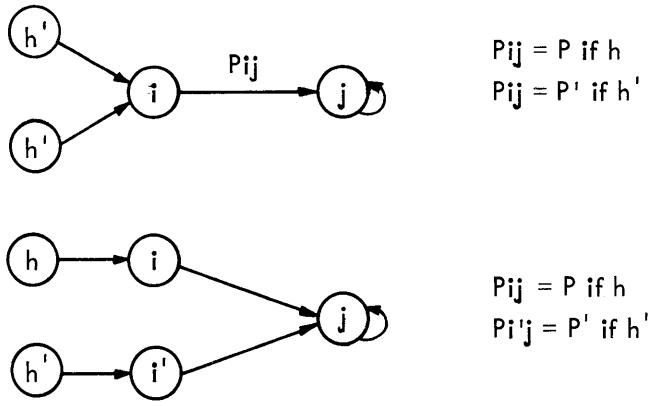

Fig. XV-9. Showing how a simple Markov chain and memory dependence can be combined.

demonstrates[1] that such a dummy state allows the experimenter an additional degree of freedom because the composite (dummy plus original) state will allow him to retain the correct mean passage time and will enable him to generate correct model variance predictions. This is done by adjusting transition probabilities of the dummy state.

A compromise must be found that maximizes the mean and variance accuracy while minimizing numerical complexity. The Markov model has a computational advantage over other models in that one considers straightforward matrix manipulation, which is well suited to computer calculation. Thus, the prospect of creating an additional state is not discouraging. Also, the equations giving the transition probabilities for the dummy states can be solved by routine numerical methods.[2]

Hence, once we define the stages in the model, based on a priori generalizations of the input data, the partitioned Markov model is quite adaptable to computer programming.

2. Relation to Human Tracking

Three generalizations concerning human tracking responses can be made. First, when a subject is in a steady nonpredicting state, if he is given a predictable waveform, he does not initially predict that waveform. Second, after a short time, his responses will lack synchronization with the target, but the responses will be frequency-dependent upon the target. Third, he will eventually predict the target waveform and his responses will show good target synchronization.

We may classify the subject's state of prediction according to the delay times between the target and the zero crossings of his response. For example, we might define the five states shown in Fig. XV-10.

The values defining the states can be arbitrary, and the model still gives consistent predictions. Nevertheless, we want parameter predictions and estimations in a model which are based on physical parameters. Thus, in practice the definitions of the

reaction-time state are based on known facts of the system under study. For example, we might define accurate eye-movement prediction as $-125 < t < +125$ msec, this range (250 msec) being a typical eye-movement sampling period.

In terms of the three previously defined adaptation stages, we may define a 3-state model. Let us say that the model has undergone transition to stage 2 (frequency-dependent tracking) when the empirical data show the first accurate prediction. Similarly, let us say stage 3 is attained only after two successive accurate predictions.

State	Definition	Range of delay times (msec)
A	nonprediction	$150 < t < \infty$
B	slight prediction	$50 < t < 150$
C	accurate prediction	$-50 < t < 50$
D	slight overprediction	$-150 < t < -50$
E	overprediction	$-\infty < t < -150$

Fig. XV-10. Possible classification of the subject's state of prediction.

Billheimer found that the inherent nature of the nonstationary tracking responses, particularly in the early stages of adaptation, required that he build memory dependence into the first stage of the model. The previously mentioned expansion and dummy-state introduction technique was used in the first stage of this model. Billheimer found that this configuration of the partitioned model gave optimum accuracy for a minimum number of states. A detailed description of the calculations involved in partitioning the model is given in Billheimer's thesis.[1]

3. Computer Program

A program to perform the data acquisition and model generation has been written[3] for the G. E. 225 computer. The computer generates a random (period and amplitude) square wave and sends this voltage to a tracking apparatus. The experimenter can switch to a periodic square-wave output of a specified frequency. The subject's response (eye movement or hand movement) is digitized with the input. Using the reaction times of the response, measured by zero crossings, the computer generates an array of reaction times in milliseconds versus period number.

When enough responses have been taken to ensure that the subject is predicting accurately, the experimenter switches to data collection and the results are written on

tape. An unlimited number of different records are allowable; therefore, a model can be generated by using data from different subjects.

The analysis program retrieves data specified by the operator and reads a card containing the reaction-time state definitions. Thus, if R runs were retrieved, and if the reactions times for the first 20 periods are to be processed, then an R × 20 array is generated (Fig. XV-11).

Run \ Period, n	1	2	3	4	5	...	20
1	A	A	C	D	C	...	E
2	A	B	B	C	B	...	D
3	A	A	A	A	A	...	E
4	A	A	C	C	B	...	C
.	.	.	.	.	.	...	.
.	.	.	.	.	.	...	.
.	.	.	.	.	.	...	.
R	A	A	B	D	E	...	E

Fig. XV-11. R × 20 array of reaction-time states.

If for the first period (n=1) all R runs show that the subject is not predicting (i.e., he is in state A), the transient-state occupancy probability for A is 1.00; for B through E is 0.00. For n = 2, if one B and (R-1) A's appear, then the probability of occupying state B is $\frac{1}{R}$, and of occupying state A is $\frac{R-1}{R}$.

Thus, we may plot five transient-state occupancy probability curves, one for each state A to E, and use these empirically calculated curves for comparison with those predicted by the model.

The program calculates six other empirical measures:

a and b; the first and second moments of the number of steps needed to exit from state A (nonprediction).

c and d; the first and second moments of the number of steps needed to enter state C.

e and f; the first and second moments of the number of states passed through before entering state C.

These statistics form the input to the model-generation algorithm. The program then generates a partitioned matrix as indicated in Figs. XV-12 and XV-13.

The size of the matrix has been fixed a priori. The computer is allowed to adjust the transition probabilities for the dummy states to give an accurate prediction of the

	A_1	A_2	B_2	C_2	D_2	E_2	A_3	B_3	C_3	D_3	E_3	Row Totals
A_1	57		13	3		4						77
A_2		46	32	12	5	5						100
B_2		36	27	7	5	14						89
C_2		7	6		6	6			14			39
D_2		4	4	10	4	20						42
E_2		8	8	9	22	32						79
A_3							4	5	4	3		16
B_3							4		7	5	2	18
C_3							6	10	28	11	9	64
D_3							2	3	8	15	9	37
E_3							1	2	6	10	14	33

Fig. XV-12a. State transitions for 0.4-cps square-wave input (afterBillheimer[1]).

	A_1	A_2	B_2	C_2	D_2	E_2	A_3	B_3	C_3	D_3	E_3
A_1	.740		.169	.039		.052					
A_2		.460	.320	.120	.050	.050					
B_2		.404	.304	.079	.056	.157					
C_2		.179	.154		.154	.154			.359		
D_2		.095	.095	.238	.095	.477					
E_2		.101	.101	.114	.278	.406					
A_3							.250	.312	.250	.188	
B_3							.222		.389	.278	.111
C_3							.094	.156	.438	.172	.140
D_3							.054	.081	.216	.405	.244
E_3							.030	.061	.182	.303	.424

Fig. XV-12b. Corresponding stochastic matrix of response model for 0.4-cps square-wave input.

	A_1	A_2	B_2	C_2	D_2	E_2	A_3	B_3	C_3	D_3	E_3	Row Totals
A_1	31		4	6								41
A_2		1	1									2
B_2		1	1	4	1							7
C_2			1		8	6			8			23
D_2				11	20	9						40
E_2				2	13	10						25
A_3												0
B_3										1		1
C_3									10	20	5	35
D_3								1	22	77	27	127
E_3									6	24	20	50

Fig. XV-13a. State transitions for 1.0-cps square-wave input, average of 10 subjects (after Billheimer[1]).

	A_1	A_2	B_2	C_2	D_2	E_2	A_3	B_3	C_3	D_3	E_3
A_1	.756		.098	.146							
A_2		.500	.500								
B_2		.143	.143	.571	.143						
C_2			.043		.348	.261			.348		
D_2				.275	.500	.225					
E_2				.080	.520	.400					
A_3										1.000	
B_3									.286	.571	.143
C_3								.009	.102	.658	.231
D_3									.120	.480	.400
E_3											

Fig. XV-13b. Corresponding stochastic matrix of response model.

same 6 input statistics mentioned above.

Given the stochastic matrix defining the model, the computer calculates predictions of transient-state probability by using these relationships:

$$\phi_{ij}(n) = \text{Prob (state n=j/state 0=i)}$$

The multistep transition probability is related to the stochastic matrix, P, of the model by

$$I(n) = p^n,$$

where I(n) represents a matrix having elements $\phi_{ij}(n)$.

Figures XV-14 and XV-15 show some models of the eye-tracking and hand-tracking responses to a 0.5-cps square wave which have been derived by the computer. Figures XV-16 and XV-17 represent Billheimer's derived curves for 0.4-cps and 1.0-cps

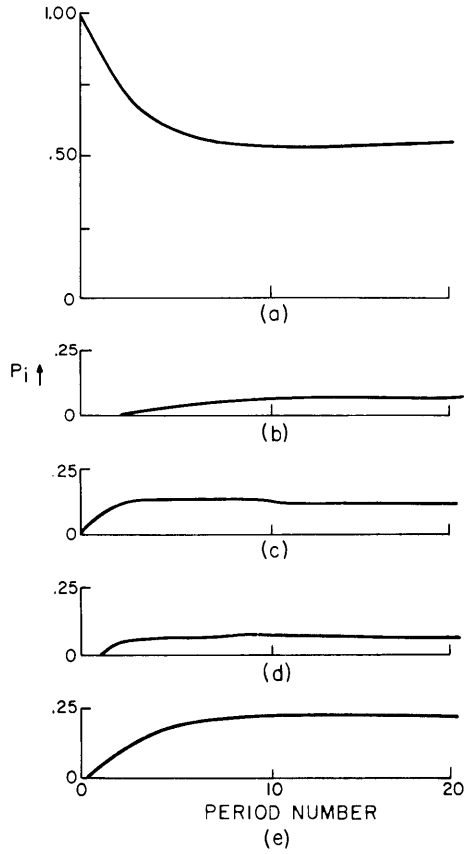

Fig. XV-14. Computer-derived transient-state occupancy probability curves for each of 5 reaction-time states. Input data are eye-tracking response to 0.5-cps square wave.

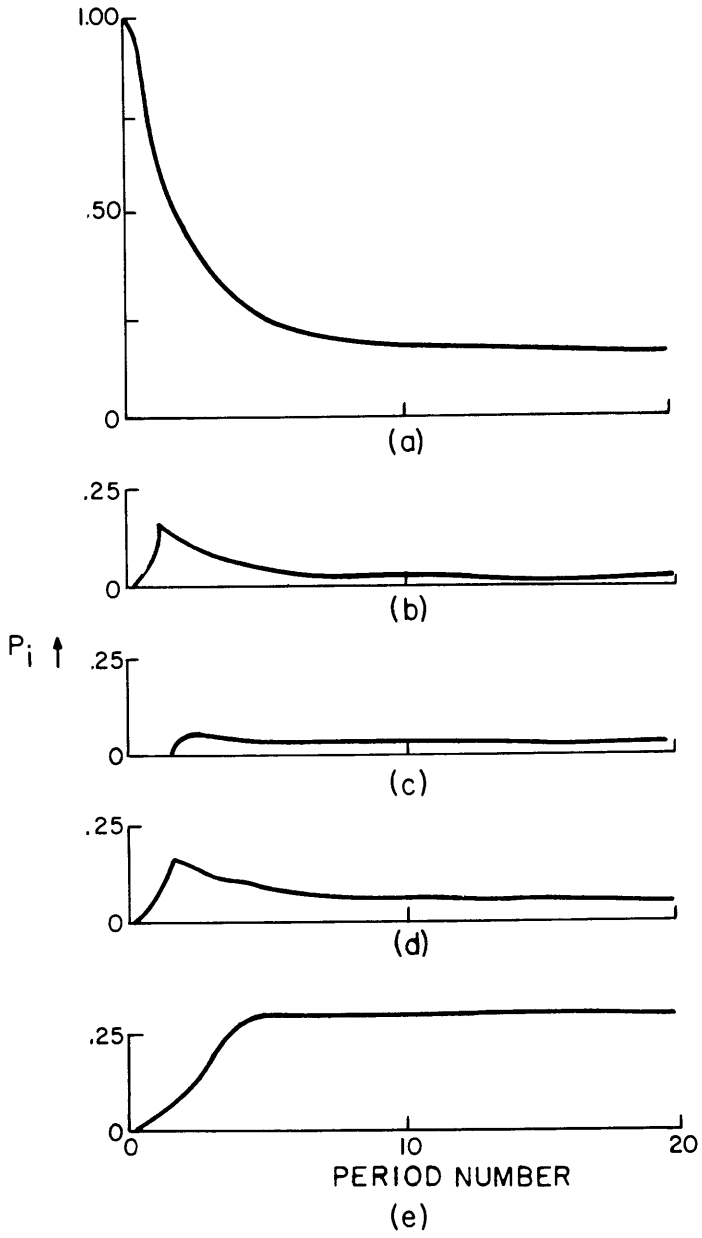

Fig. XV-15. Corresponding curves for hand-tracking response to 0.5-cps square wave.

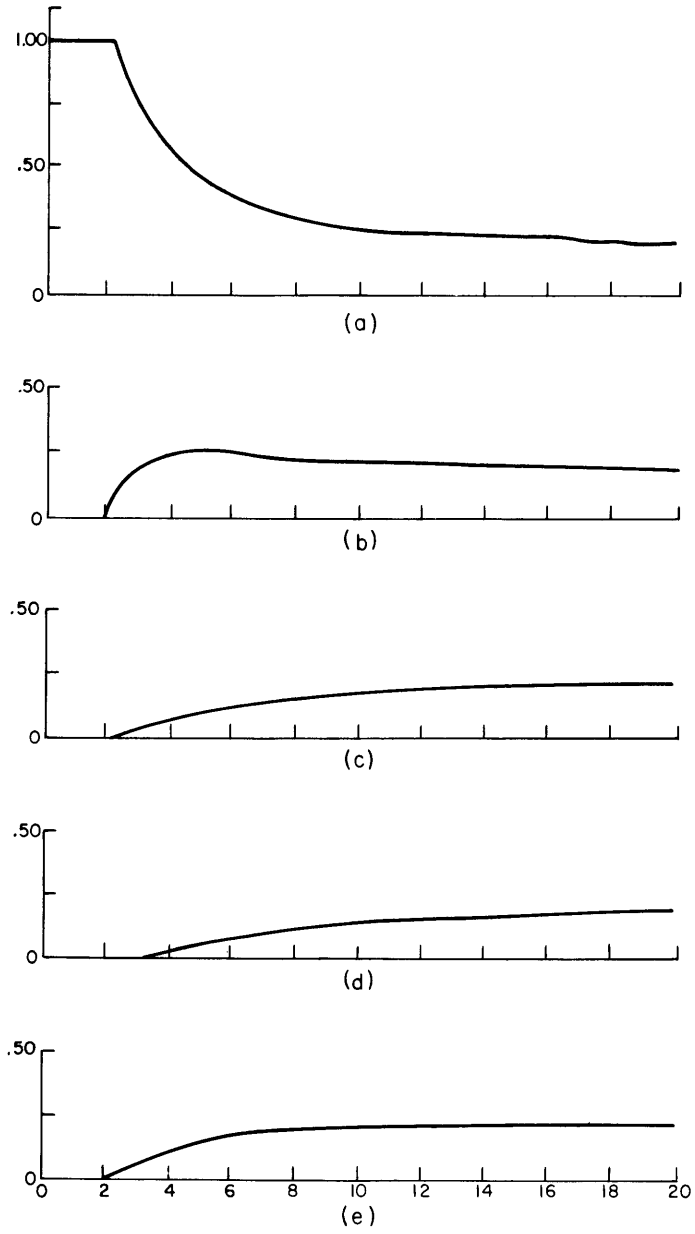

Fig. XV-16. Transient-state occupancy probabilities for each of 5 reaction-time states. Curves derived from 0.4-cps square-wave model (after Billheimer[1]).

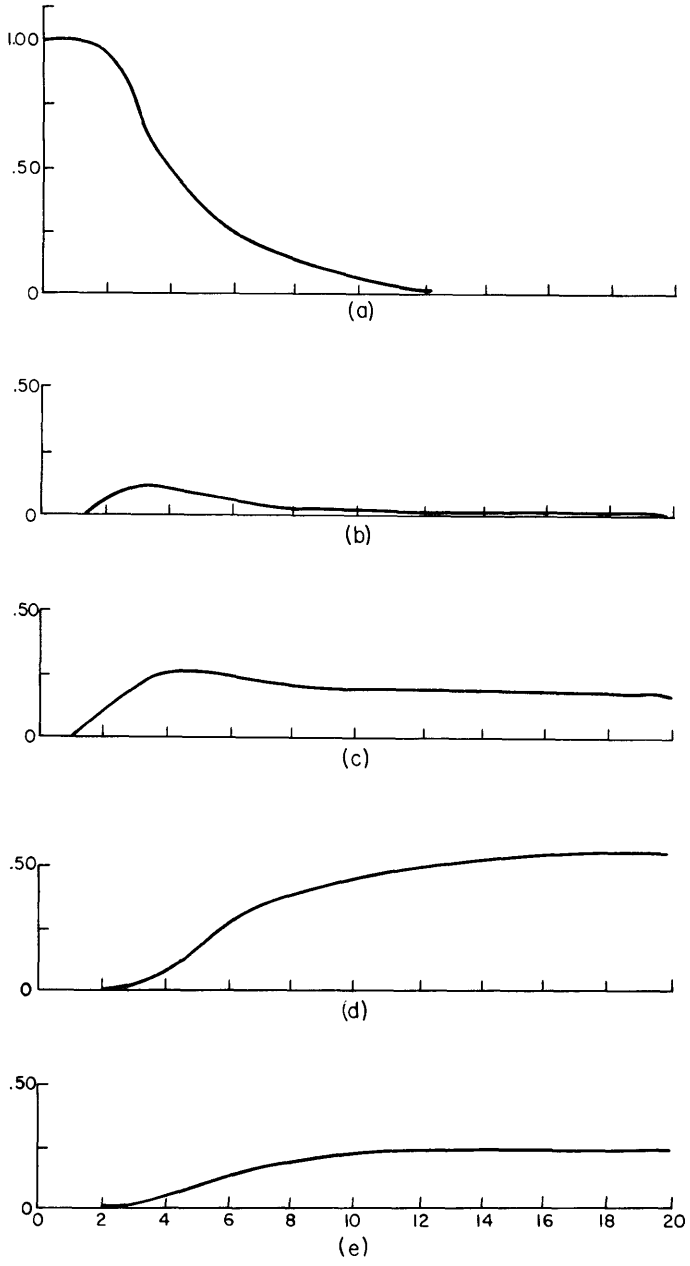

Fig. XV-17. Transient-state occupancy probabilities for the same 5 reaction-time states. Response derived from 1.0-cps square-wave model (after Billheimer[1]).

square-wave inputs to the hand-tracking system. These plots are based on the stochastic matrices given in Figs. XV-12 and XV-13, respectively.

Computer verification of the partitioning techniques is still in an early phase, but preliminary results[4] demonstrate that the partitioned Markov model exists in a mathematical

framework that is fully capable of allowing analysis of adaptive tracking patterns.

G. A. Masek, L. Stark

References

1. J. W. Billheimer, A Markov Analysis of Adaptive Tracking Behavior, E.E. Thesis, Department of Electrical Engineering, M.I.T., September, 1963.

2. J. Kemeny and J. Snell, Finite Markov Chains (D. Van Nostrand Company, Inc., Princeton, New Jersey, 1960).

3. N. Barnett, A Markov Model by Program, Arcon Co., 1963 (unpublished).

4. G. Masek, The Sampling Process in Human Visuo-Motor Tracking, S.M. Thesis, Department of Electrical Engineering, M.I.T., September, 1964.

D. SACCADIC SUPPRESSION

In a previous report the time course of saccadic suppression relative to the time course of a 20° saccadic eye movement was published.[1] A figure representing this phenomenon graphically is shown in amended form as Fig. XV-18. It will be noted that

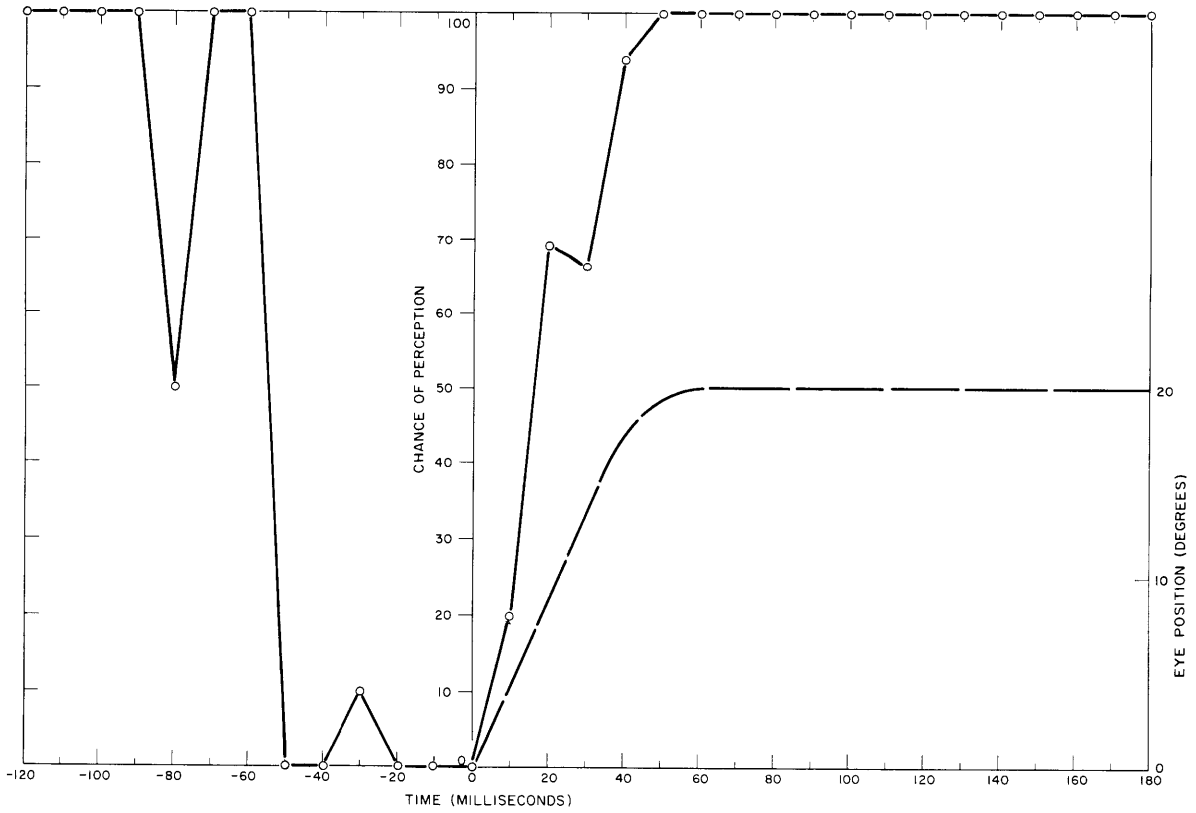

Fig. XV-18. Saccadic suppression during voluntary saccadic eye movements.

the schematic representation of the time course of the eye movement has been changed. This change has been prompted by the discovery of a dynamically limiting electronic element (filter) that shaped our eye-movement recordings and made them appear to last longer than was actually the case. The true duration of a 20° saccade is 40-50 msec (see Fig. XV-18). For reference, an accurate recording of a typical 20° saccade is shown in Fig. XV-19.

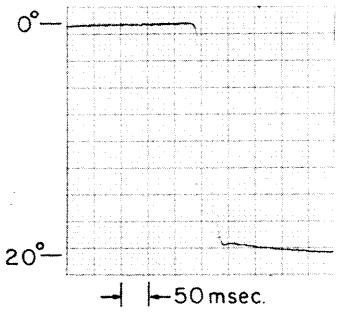

Fig. XV-19. A typical 20° saccade.

It would appear that, in these experiments, the portion of the saccadic suppresion phenomenon that follows the onset of the eye movement has a time course roughly similar to that of the eye movement. Thus, the chance of perception has returned to 100 per cent at approximately the same time that the eye movement has terminated (40-50 msec). It is important to remember that the dynamically limiting element had no effect on the time course of saccadic suppression, since, for analysis, this phenomenon was related to the beginning of the eye movement.

B. L. Zuber

References

1. B. L. Zuber, J. A. Michael, and L. Stark, Visual suppression during voluntary saccadic eye movements, Quarterly Progress Report No. 74, Research Laboratory of Electronics, M.I.T., April 15, 1964, pp. 217-221.

E. ADAPTIVE CONTROL OF THE ARTERIAL SYSTEM: LUMPED-PARAMETER TRANSMISSION-LINE ANALYSIS

Adaptive control refers to those systems that change their characteristics in response to extreme parameter changes in the system or to major external disturbances, and thereby optimize their performance. This adaptation involves the automatic correction of some part of a system in order to correct for variations in system dynamics. In the design of such a system, a figure of merit or reference that will provide optimum performance must be determined. The system must continuously compare the actual performance with the reference performance and must automatically adjust its parameters to minimize the difference between the desired and actual performance. It is reasonable that experimental studies from the biological area may contribute to further understanding of adaptive control. The qualitative control features of the cardiovascular system suggest that it is a suitable area for an investigation of adaptive control.

The behavior of the arterial system can be considered analogous to an electrical transmission line. By the analysis of a segment of this line as a lumped-parameter network, the arterial parameters may be calculated from measurements of pressure, flow, and distention of the vessel wall. Computer analysis of these data yields the variation of the parameters with time and allows insight into some of the primary feedback features of the cardiovascular control mechanism and into the adaptive dynamic behavior of the arteries under the influence of systemic disturbance. A question arises whether the lumped-parameter network, which is chosen for its computational advantages, is as good an analog of the arterial segment as the distributed-parameter transmission line on which it is based. This necessitates an analysis of the error resulting from this approximation and a comparison with the accuracy of the in vivo physiological experiments.

In the determination of an electrical transmission line that is analogous to an arterial segment, one makes the following primary assumptions. (i) The blood is Newtonian, that is, the viscosity is not dependent on sheer. Blood does not have this property but the approximation is appropriate for the arterial segment. (ii) The rate of flow of blood is not a function of time. (iii) The flow of blood is laminar, and thus there is no component of flow perpendicular to the axis of the tube. (iv) The blood does not slip at the wall, that is, the outermost layer of blood has zero velocity. (v) The artery is long compared with the segment under study so that unusual conditions at the inlet or outlet have no influence on the flow. (vi) The artery is so rigid that the diameter is not a function of pressure.

For blood flow in the arterial segment, one can write a force equation for the motion of the blood. This equation must be reconstructed to remove the assumption of steady flow. The generalized relationship between the pressures of a fluid and the fluid velocity is dependent on the fluid density and viscosity, and this can be described by the Navier-Stokes equation. If this relation is expressed in cylindrical coordinates, and if it is assumed that the driving pressure gradient can be represented as a harmonic series, the result is a Bessel equation. The solution gives the fluid velocity. Integration of this velocity over the cross section of the tube yields the flow. For any given frequency, the flow may be separated into a component in phase with the pressure gradient and a component in quadrature with it. Consequently, a distributed inductance and resistance can be assigned to the fluid. The hydrodynamic behavior of the blood thus contributes an LR series branch to the transmission-line analog.

For the arterial wall undergoing strain, its tension can be expressed essentially by the equation for a mass-spring system with viscous damping. Here the radial flow can be expressed as the time rate of change of volume caused by wall distention. The wall tension can be related to the pressure within the vessel by equating the forces of each which act on the arterial wall. Substitution of this relationship in the expression for the mass-spring system yields a pressure-flow equation for the arterial wall which is analogous to the voltage-current relationship in an RC series branch. Thus, the

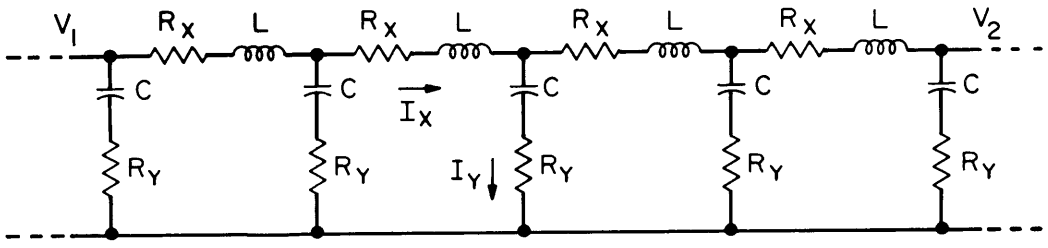

Fig. XV-20. Transmission-line analog of blood-filled arterial segment.

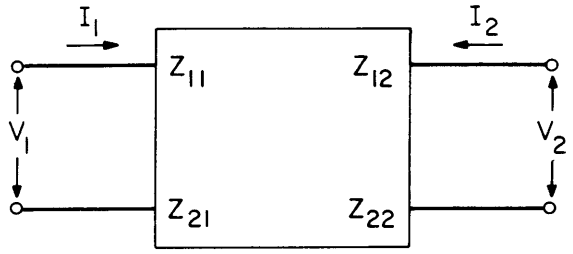

Fig. XV-21. Generalized two-port network.

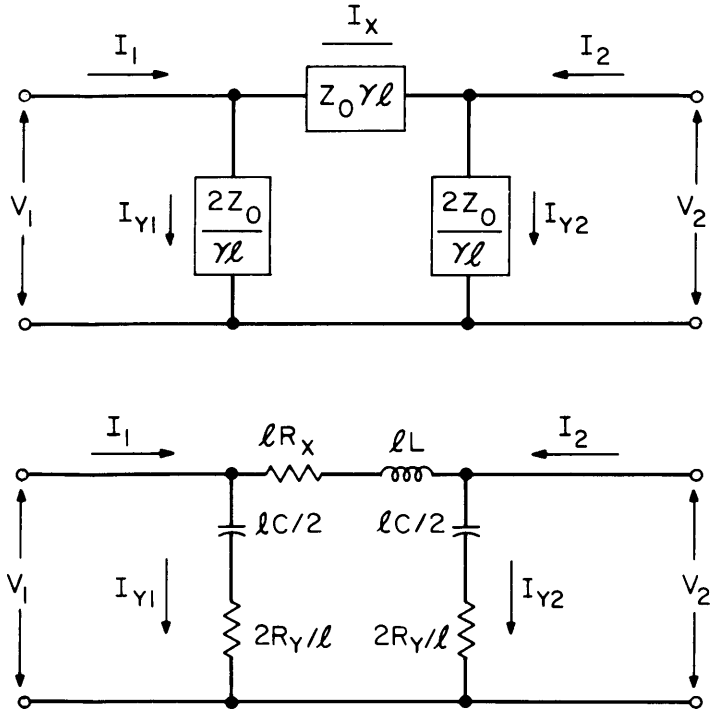

Fig. XV-22. Representation of arterial segment as a lumped-parameter network.

distributed shunt-admittance portion of the analogous transmission line comprises a distributed RC branch.

A similar analysis for the dynamic equations describing the behavior of the arterial blood flow and the arterial wall results in the basic configuration for the electrical analog shown in Fig. XV-20. The distributed electrical parameters of this transmission line represent the following mechanical properties of a blood-filled arterial segment: R_x represents the viscous drag resistance of the blood, L represents the mass of the blood, R_y represents the viscoelastic resistance of the arterial wall, and C represents the elastic compliance of the arterial wall.

Although the arterial system is structurally complex and the arterial dimensions and the wall moduli vary from area to area, some segments of the abdominal aorta of the dog have properties that are uniform and encompass no discontinuities. The relative uniformity of these segments makes them suitable for analysis with an analogous electrical transmission line having uniformly distributed parameters.

In dealing with short segments of an artery, the transmission line can be approximated by a lumped-parameter network. This approximation provides some computational advantages and allows a description of the mechanical behavior of an artery to a certain extent. Nevertheless, one must consider the error incurred in this lumped-parameter approximation.

A section of transmission line that is part of a more complex network can be regarded as a two-port network that transforms the output (V_1 and I_1) of the preceding line segment into the input (V_2 and I_2) of the following segment as indicated in Fig. XV-21. The generalized equations describing such a two-port network are

$$V_1 = Z_{11}I_1 + Z_{12}I_2$$

$$V_2 = Z_{21}I_2 + Z_{22}I_2.$$

For the particular case in which the two-port network is known to be a transmission line of length ℓ, propagation constant γ, and characteristic impedance Z_o, the input and output impedances (Z_{11} and Z_{22}) can be written

$$Z_{11} = Z_{22} = Z_o(\coth \gamma\ell) \tag{1}$$

and the transfer impedances (Z_{12} and Z_{21}) are

$$Z_{12} = Z_{21} = Z_o/(\sinh \gamma\ell). \tag{2}$$

With these relationships it is possible to compute γ and Z_o from the simultaneous measurements of V_1, I_1, V_2, and I_2 (which are analogous to the input and output pressures and flow in the arterial segment). If γ and Z_o were known for any frequency

components of the pulse wave, then the arterial parameters (R_x, R_y, L and C) could be computed by using the expression for the propagation constant

$$\gamma = \sqrt{\frac{R_x + j\omega L}{R_y - j/\omega C}},$$

and for the characteristic impedance

$$Z_o = \sqrt{\frac{Z}{Y}}.$$

Although the expressions for γ and Z_o are far easier to deal with than those for the apparent phase velocity and attenuation, the computations involved to obtain values for the arterial parameters would still be unnecessarily complex. The computational difficulties are largely attributable to the distributive nature of the transmission line. This gives rise to the hyperbolic functions sinh $\gamma\ell$ and coth $\gamma\ell$ in Eqs. 1 and 2.

The use of a lumped-parameter network can considerably simplify the computations by making it possible to calculate the arterial parameters directly from measurements of flow and pressure. Although it is recognized that a distributed-parameter transmission line can never be completely described by lumped parameters, the approximation becomes quite accurate when the length of the segment is small compared with the wavelength of the highest significant harmonic in the arterial pulse. In this instance, the arterial segment can be represented by a lumped-parameter pi-network as shown in Fig. XV-22. The two-port network impedances for this circuit are

$$Z_{11} = Z_{22} = \frac{Z_o[1+(\gamma\ell)^2/2]}{\gamma[1+(\gamma\ell)^2/4]} \tag{3}$$

$$Z_{12} = Z_{21} = \frac{Z_o}{\gamma[1+(\gamma\ell)^2/4]}. \tag{4}$$

The analysis of error resulting from this approximation (that is, the use of Eqs. 3 and 4 to represent Eqs. 1 and 2) has been treated by Vierhout.[1] The application of this type of analysis indicates that the errors of approximation e in Z_{11}, Z_{12}, Z_{21} and Z_{22} are all given by

$$e = -\frac{(\gamma\ell)^2}{12}.$$

From the expression for the propagation constant

$$\gamma = \sqrt{\frac{R_x + j\omega L}{R_y - j/\omega C}}$$

it is seen that

$$\gamma^2 = \frac{(R_x + j\omega L)}{(R_y - j/\omega C)}$$

which becomes

$$\gamma^2 = \left[\frac{1}{R_y^2 + (1/\omega C)^2}\right]\left[\left(R_x R_y - \frac{L}{C}\right) + j\left(\omega L R_y + \frac{R_x}{\omega C}\right)\right].$$

The real component of this expression represents the amplitude error, and the imaginary component represents the phase error. Both components increase with frequency and, hence, the greatest error occurs for the highest significant harmonic in the pulse wave. To estimate the maximum error to be expected when the pi-network is used, an upper frequency limit of 30 cps is assumed. (This limit represents the tenth harmonic of a pulse rate of 180 per minute.) This is a fairly conservative figure, since the highest harmonic that can be recorded with any accuracy (i.e., that will be significantly above the noise level) has been generally found to be well below 30 cps. By using numerical values arrived at by others[2-4] for blood viscosity and density, arterial wall elastance, viscoelastance, thickness, and radius, typical values for the arterial parameters R_x, R_y, L, and C can be computed. For the values chosen (based on a representative segment of abdominal aorta), the computed value of γ^2 for a frequency of 30 cps is

$$\gamma^2 = (-0.00103 + j.00600).$$

For the in vivo data of a segment of artery 10 cm in length ℓ the resultant error becomes

$$e = -\frac{(100)}{12}(-0.00103 + j.00600) = 0.0086 - j.055).$$

This means that the maximum error (in Z_{11}, Z_{12}, Z_{21} and Z_{22}) resulting from the pi-network approximation is less than 1 per cent in amplitude, and approximately 3° (0.055 radian) in phase. The errors for the lower harmonics are even smaller. These errors are far less than the accuracy that is possible for in vivo physiological experiments, and thus the errors can be neglected.

Consequently, for the analysis of the adaptive dynamic behavior of arteries under the influence of systemic disturbances, the lumped-parameter pi-network analog of the arterial segment is as good as the distributed-parameter transmission line analog.

J. F. Dickson III

References

1. R. R. Vierhout, Approximate models for transmission lines and their error, Electronic Eng. 31, 94 (1959).

2. D. A. McDonald and M. G. Taylor, The hydrodynamics of the arterial circulation, Progr. Biophys. 9, 107 (1959).

3. L. H. Peterson, R. E. Jensen, and J. Parnell, Mechanical porperties of arteries in vivo, Circulation Res. 8, 622 (1960).

4. D. L. Fry, The measurement of pulsatile blood flow by the computed pressure-gradient technique, IRE Trans., Vol. ME-6, p. 259, 1959.

F. PHOTOSENSITIVE NEURONS OF THE CRAYFISH SIXTH GANGLION AS A DUAL SYSTEM, EACH NEURON CARRYING THE SAME SIGNAL INFORMATION

Studies on the nerve-impulse patterns from the two photosensitive neurons of the sixth abdominal ganglion of the crayfish have been reported previously.[1]

In this report we present evidence that the signals carried by each of the two photoreceptors elicit the same walking-movement response of the legs. The new results reinforce our view that the code carried by each fiber passes through the same decoding mechanism.

In our previous results, the absence of correlation in the detailed pattern of the sequences of intervals between nerve impulses of the two parallel nerve trains that come from the photoreceptor was demonstrated by visual comparison of the two nerve impulse trains, and also by histograms of the interval between a pulse in one fiber and the next pulse in the other fiber. These histograms were linear on a semi-logarithmic scale, as they would be if the two fibers were uncorrelated and produced a Poisson distribution of these interfiber intervals.

We now present further evidence in the form of interval histograms and of autocorrelation and crosscorrelation functions to substantiate the absence of correlation noted previously, and to give a quantitative estimate of some minor correlations that occassionally appear.

1. Method

The dissection, the recording of the pulse trains, and the mechanical recording of the leg movements have been extensively described in previous reports.[1-3]

2. Results

a. Walking-Movement Response

Figure XV-23 shows that hemisection of the ventral ganglionic chain does not suppress the walking-movement response. The preserved response is similar in both sides

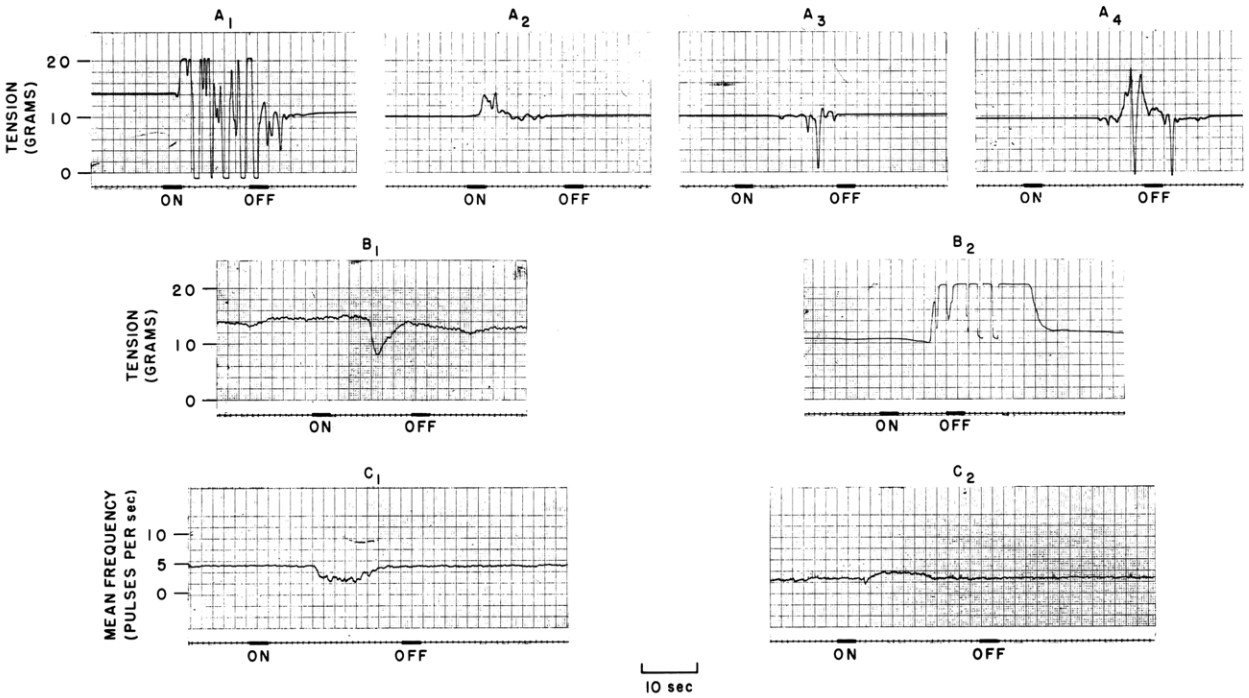

Fig. XV-23. Walking responses produced by light stimulation of the sixth abdominal ganglion of the crayfish. Part A, tension produced by the movement of a walking leg during light stimulation. A_1 and A_2, before; A_3 and A_4, after hemisection of the ganglionic chain. Notice the increased latency of the response in A_3 and A_4. Part B, tension recording of the walking response with the ganglionic chain intact. B_1, pure extensor response. B_2, flexor response in the same preparation. Part C, average frequency of the motor nerve pulse train during light stimulation. C_1, inhibitory effect. C_2, excitatory effect in the same preparation. Note that a positive signal (increased average frequency rate) in an early part of the system (ventral nerve cord) causes both excitation and inhibition in a later part (motor nerve, C_1) and flexion and extension of the output element (leg tension, B_1).

of the animal and only an increase in the latency of response is observed.

In Fig. XV-23, responses can be noted with alternating flexion and extension movements (A), mainly flexion movements (B_2), and purely extension movements (B_1). When the average frequency of the discharge of the motor neurons of the leg muscles was recorded, we found that the response consisted mainly of either an increase (C_2) or a decrease in the average frequency (C_1).

b. Fibers Showing No Correlation

The pulse trains from the two photoreceptor cells were recorded simultaneously under constant light stimulation. The light-intensity information is transmitted at the main firing frequency, which is approximately the same in both fibers, as shown in the interval histograms (c) of Fig. XV-24c. The highly periodic characteristics of the firing pattern are reflected in the periodic features of the autocorrelation functions in Fig. XV-24b. Nevertheless, it is clear from FIg. XV-24a that the crosscorrelation functions do not show significant deviations from the mean. We feel that this is the crucial experimental result.

c. Fibers Showing Minor Correlations

Occasionally, minor correlations were observed, statistically significant with these averaging techniques, but not strong enough to revive the idea of the detailed-pattern code with a high information rate. An example of minor correlation is shown in Fig. XV-25 which also shows the highly periodic autocorrelation functions (Fig. XV-25b). Here, however, the crosscorrelation function (Fig. XV-25a) shows periodicities that extend beyond the ±2 standard-deviation lines on the graphs. The most significant peak in Fig. XV-25a, at $\tau = 0$, represents a negative correlation of −3.3 pulses/sec as compared with the 44 pulses/sec average rate and 9.2 ± 0.6 pulses/sec chance coincidence rate, which is determined by the grid size (2 msec) chosen for coincidences.

The possibility that this periodic fluctuation resulted from a periodic error in the crosscorrelation computation suggested a "control experiment" wherein we compared two impulse trains from different crayfish, but with quite similar average frequencies. The result is shown in Fig. XV-26 and the crosscorrelation function stays well bounded by the ±2 standard-deviation lines as expected (Fig. XV-26a). It is important to note that although the autocorrelation functions have strong periodicities, (Fig. XV-26b) this alone is not sufficient to produce significant crosscorrelations.

In Fig. XV-27 a collection of experimental results shows noncorrelations (Fig. XV-27b and 27d), as well as minor correlations (Fig. XV-27a and 27c); light and dark conditions are included, as well as another control (Fig. XV-27e).

Figure XV-28 shows the frequency of occurrence of the significant crosscorrelation points found in our experiments. With the preparation in darkness (Fig. XV-28a) positive

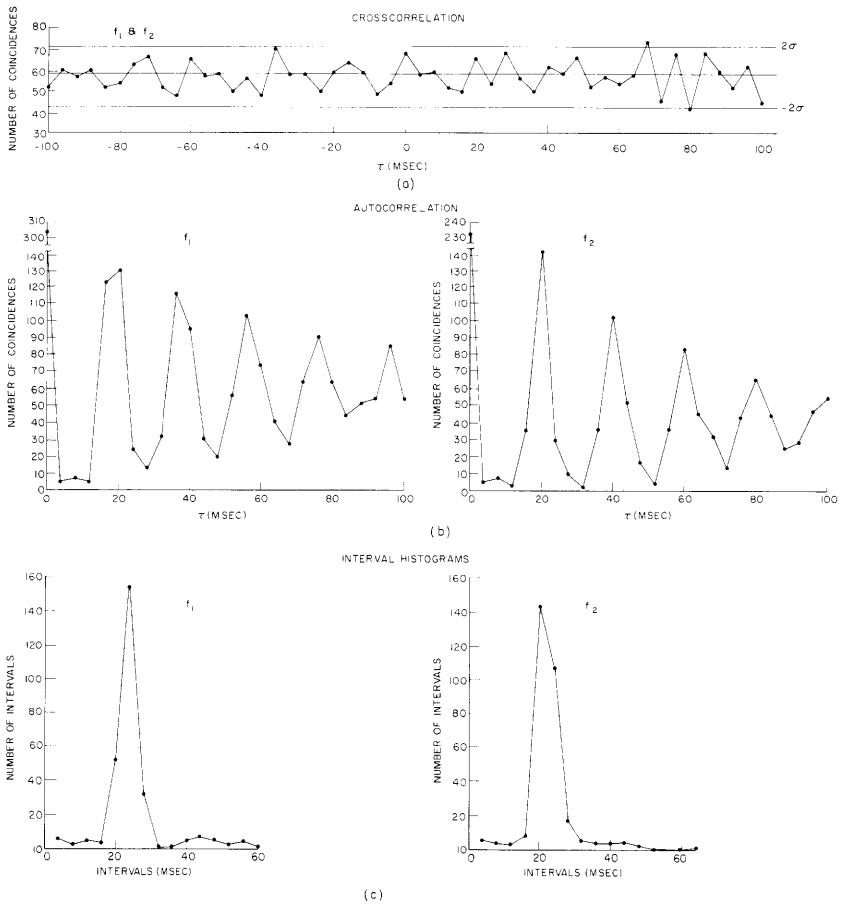

Fig. XV-24. Absence of correlation between the two nerve pulse trains coming from the photosensitive cells of the sixth abdominal ganglion of the crayfish, stimulated by steady and continuous illumination. (a) Crosscorrelation function. Note that the deviations from the mean are bounded by the two standard deviation lines of the figure. (b) Autocorrelation functions of the pulse trains of each of the two fibers (f1, f2). (c) Interval histograms of the pulse trains of each of the two fibers (f1, f2). Notice in (b) and (c) that both fibers are highly periodic and have approximately the same average interval (20 msec for fiber f1, and 26.1 for fiber f2).

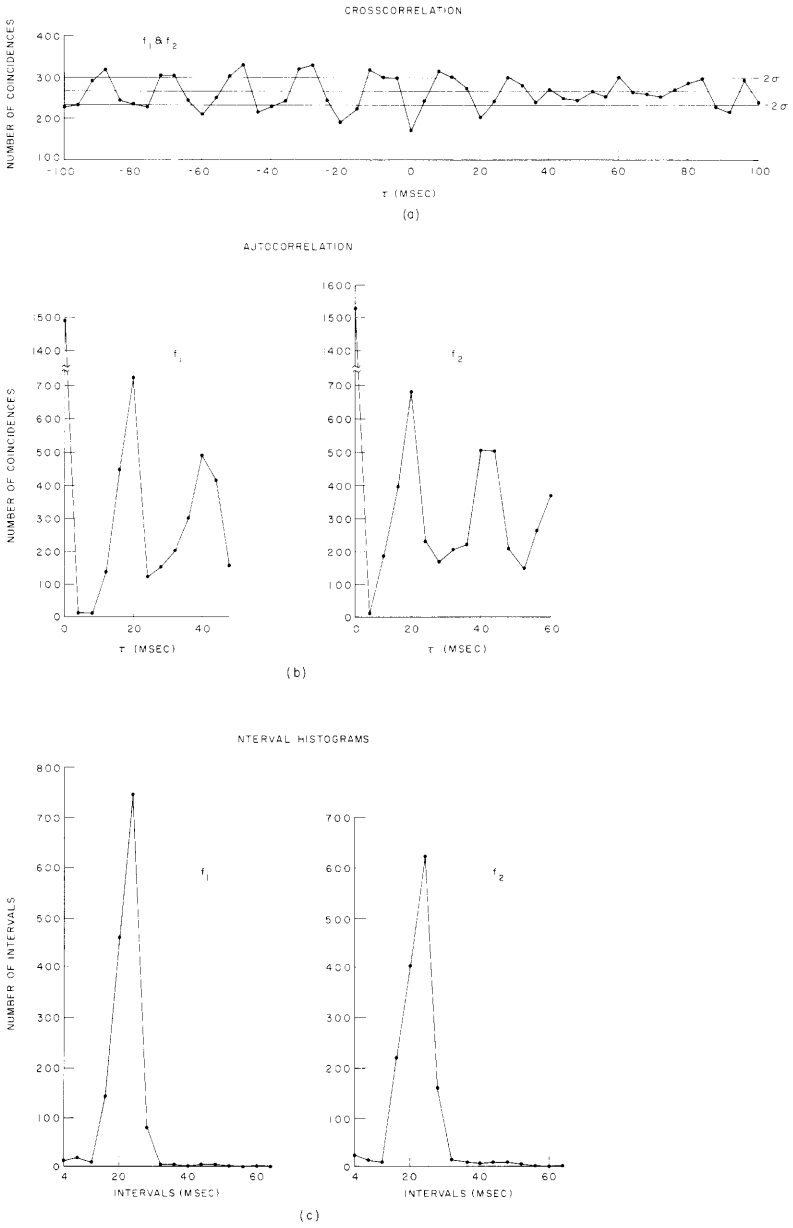

Fig. XV-25. Example of minor correlation between the two nerve pulse trains from the photosensitive cells of the sixth abdominal ganglion stimulated by steady and continuous illumination. (a) Crosscorrelation function. Notice that the deviations from the mean go above and below the two standard deviation lines drawn in the figure, in an oscillatory fashion with a period of approximately 20 msec. (b) Autocorrelation functions of the pulse trains of each of the two fibers (f1 and f2). (c) Interval histograms of the pulse trains of each of the two fibers (f1 and f2). Notice in (b) and (c) that both fibers are highly periodic with a very close average interval (20.1 msec for fiber f1, and 20.0 for fiber f2).

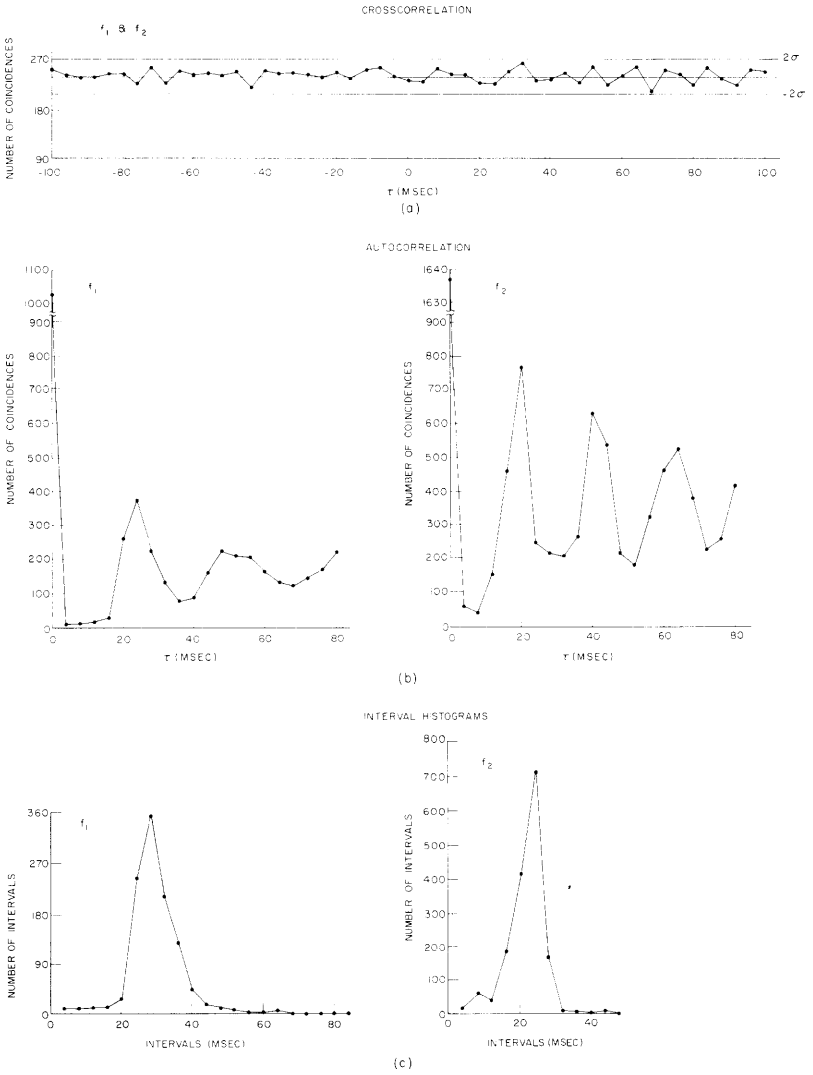

Fig. XV-26. Correlation between fibers taken from different crayfish. (a) Crosscorrelation function. Notice that the deviation from the mean is bounded by the two standard deviation lines of the figure. (b) Autocorrelation functions of the pulse trains of each of the two fibers (f1, f2). (c) Interval histograms of the pulse trains of each of the two fibers (f1, f2). Notice in (b) and (c) that both fibers are highly periodic, with a very close average interval.

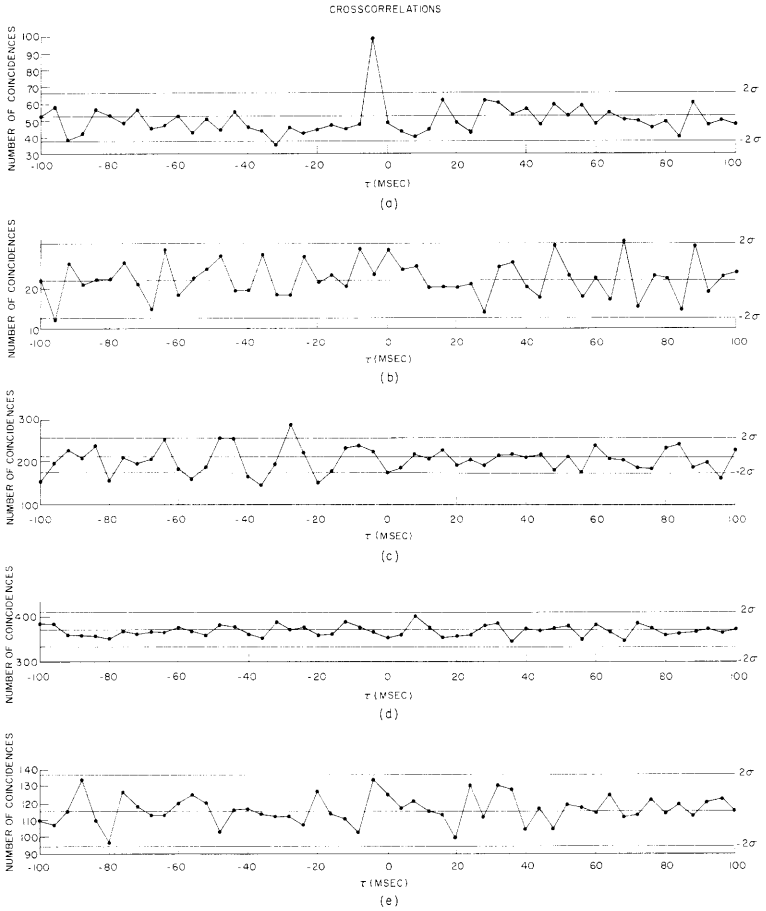

Fig. XV-27. Collection of representative crosscorrelation results. (a) Crosscorrelation with significant peak at $\tau = -4$, with two fibers in darkness. (b) Example of noncorrelation between the two fibers in darkness. (c) Experiment with some peaks and valleys of significant correlation, and some periodicity during light stimulation. (d) Clear-cut experiment showing uncorrelated fibers during light stimulation. (e) Crosscorrelation function with no significant deviations of fibers from two different crayfish ("control experiment").

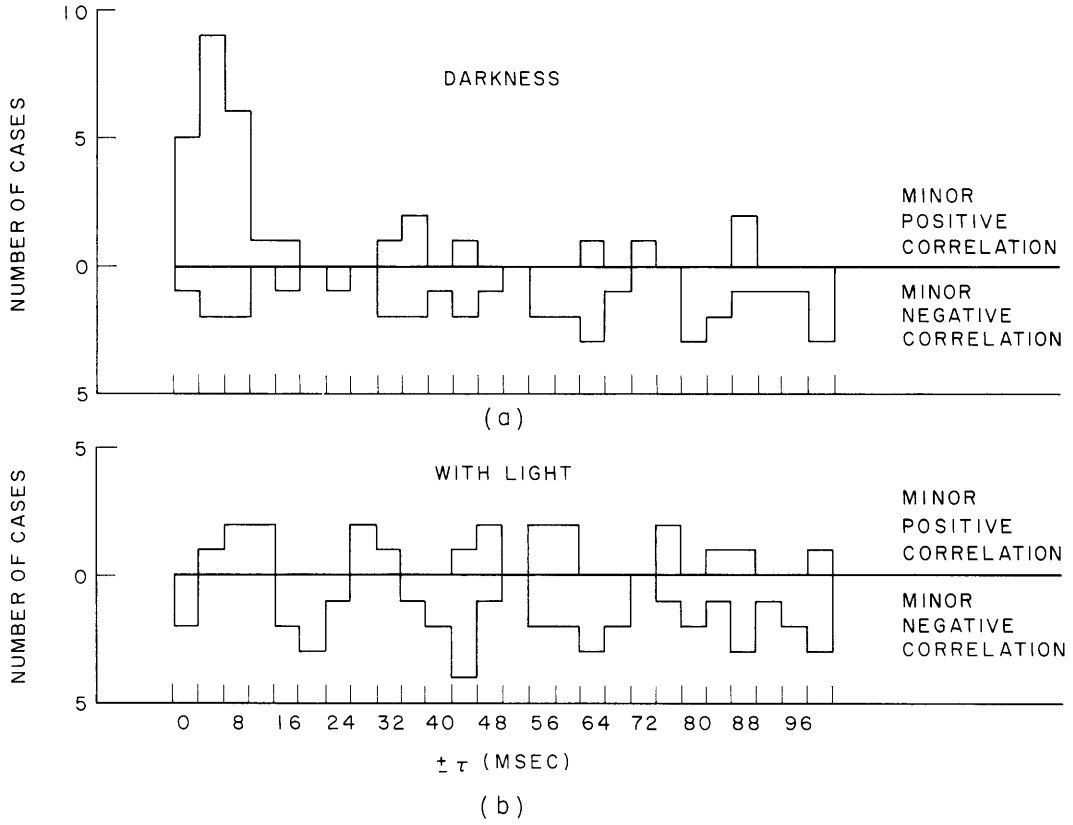

Fig. XV-28. Frequency of occurrence of the significant crosscorrelation points. Notice that with the preparation in darkness positive correlations appear at 0, ±4, and ±8 msec τ shifts. Notice that with light stimulation there is a periodicity in the beginning which fades at higher values of τ.

correlations appear at 0, ±4, and ±8 msec τ shifts frequently enough to be noticed. During light stimulation (Fig. XV-28b) there is a clear periodicity at the beginning which fades somewhat at higher values of τ. This observation agrees with the individual cases discussed above.

Figure XV-29c shows the broad and bimodal interval histograms for one unstimulated case. Accordingly, the autocorrelation functions (Fig. XV-29b) show little periodic structure. The crosscorrelation (Fig. XV-28a) shows minor but statistically significant peaks and valleys. The highest peak at -4τ represents a positive correlation of 0.7 pulses/sec, which may be compared with the 15 pulses/sec average rate and the 0.9 ± 0.2 pulses/sec chance coincidence rate (determined by the 2-msec grid size chosen for coincidences).

3. Discussion

An essential experiment was performed to establish that the two light-sensitive cells transmit the same information and therefore independently produce the same walking

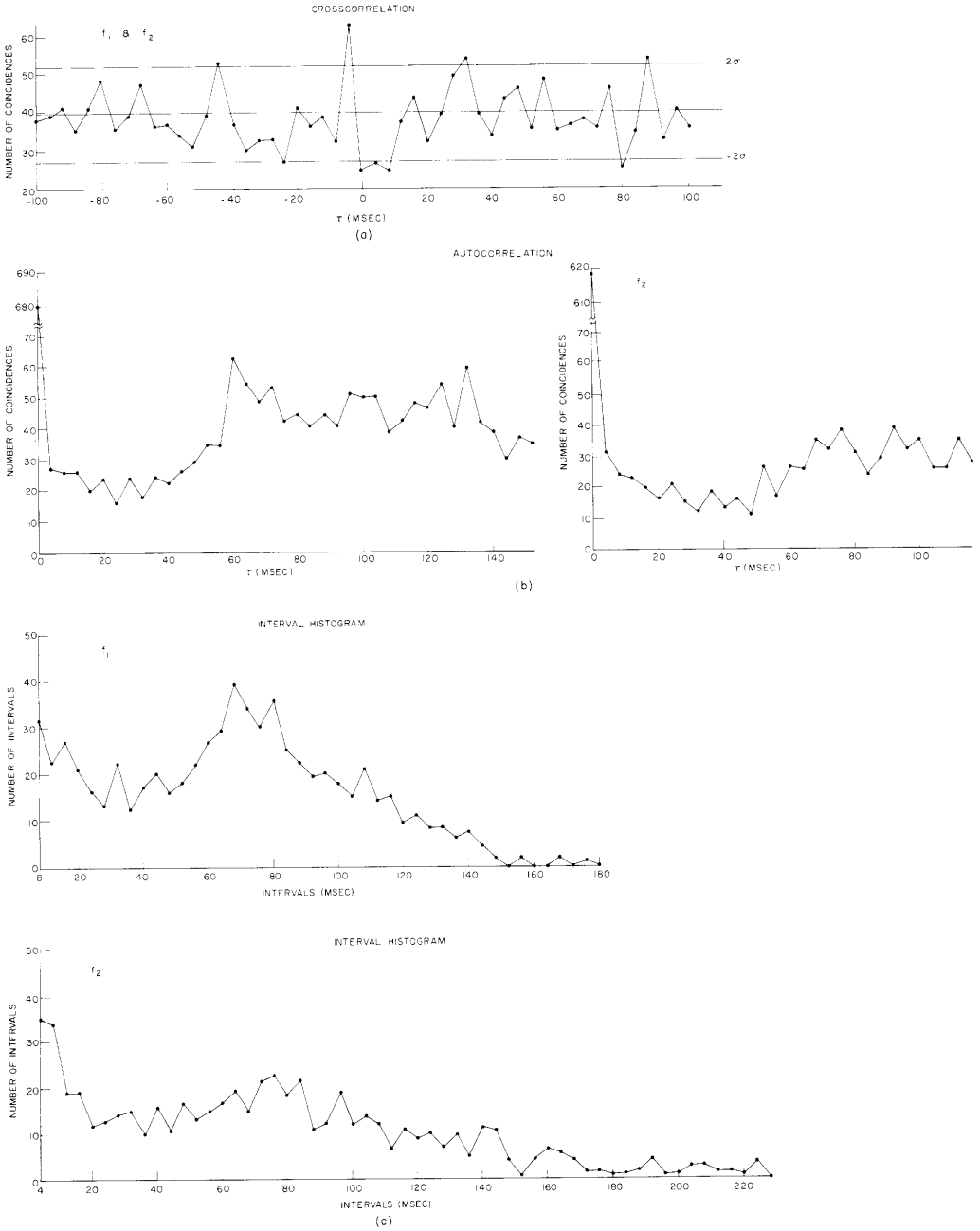

Fig. XV-29. An example of minor correlation between two nerve pulse trains coming from the photosensitive cells of the sixth abdominal ganglion in darkness. (a) Crosscorrelation function. Notice that the deviations of the mean extend above and below the two standard deviation lines at -44, -23, -4, 0, 4, 8, 32, 80, and 88, of the τ msec shift. (b) Autocorrelation functions of the pulse trains of each of the two fibers (f1 and f2). (c) Interval histograms of the pulse trains of each of the two fibers (f1, f2).

movements after one of them is illuminated. Indeed, the hemisection of the ganglionic chain does not suppress the walking response and only produces an increase in the latency of the response (Fig. XV-23a).

Our results show that both fibers convey the same information to the decoder, and it is therefore reasonable to assume that the same code must be used by the two signals. If the code is the exact timing of the pulses, then the detailed pattern of the two pulse trains should be very closely correlated. Our results seem to be crucial in this respect because no correlation has been observed and only inconsistent minor correlations have been found.

Different approaches have previously been used to investigate the detailed pattern in a nerve pulse train as a carrier of useful information. One method has been to examine the response of a cell to different patterns of controlled input nerve impulses. It has been reported that in Aplisia ganglion cells[5-7] and in the neuromuscular preparations of crustacea[8,9] pulse sequences with the same mean frequency evoke different responses that depend on the input pulse pattern. In another approach[10] the probability of "post impulse firing" in a single neuron was examined and it was argued that, since the intervals are neither Poisson distributed nor independently distributed, they convey useful detailed-pattern information.

It has been pointed out[11,12] that the use of the detailed pulse pattern as a code can provide a much higher information capacity than other coding systems. The maximum information contained in a unit of time with a code that has n symbols with a probability, P_j, for each of them and average symbol duration, b, is (see Shannon[13])

$$C = -\frac{1}{b} \sum_{j=1}^{n} P_j \log_2 P_j. \tag{1}$$

Under the simplifying assumption that the n symbols are equally frequent, we have

$$C = \frac{\log_2 n}{b}. \tag{2}$$

We would like to compare the capacity of a pulse-pattern code with that of an average-frequency code by using crayfish nerve signal characteristics. The observed intervals usually range from 10 msec to 100 msec. Thus if we assume that the system might distinguish intervals with a precision of approximately 5 msec, we have $n \approx 20$. It should be noted that these arbitrary asumptions cannot influence the results strongly, since n appears only logarithmically in the formula. Taking the average symbol duration b to be approximately equal to 50 msec we have

$$C = \frac{\log_2 20}{0.050} \approx 100 \text{ bits/sec.} \tag{3}$$

Also, it may be noted that the assumptions made in calculating the capacity of the detailed-pattern code are very conservative. Wall, Lettvin, McCulloch, and Pitts, and McKay and McCulloch, with somewhat different assumptions based on different preparations, derived rates more than one order of magnitude higher.

Let us now examine the capacity of the code based on the average frequency. Again, the frequency is found to vary from approximately 10 to 100 pulses/sec. If we assume that the decoder can distinguish levels 5 pulses/sec apart, we have approximately 20 symbols and thus, n = 20.

We must now decide what can be considered as the average duration of a symbol. It seems reasonable to assume that the system can establish the average firing frequency for a time approximately equal to its time constant. Stark and Hermann[14] obtained the transfer function of the system.

$$G(s) = \frac{32e^{-1.0s}}{(1+1.2s)^2} \qquad \text{pulses sec}^{-1} \text{ millilumen}^{-1}. \tag{4}$$

The time constant is approximately 1.2 and thus b ~1.2 sec. We finally have

$$C = \frac{\log_2 20}{1.2} \approx 3 \text{ bits/sec.} \tag{5}$$

The capacity of this average-frequency code is thus more than one order of magnitude lower than for the case in which the detailed pattern is the information carrier.

If the variance is considered as a possible signal, we see that b, the average symbol duration, must be at least as long as that specified for the mean. Thus, at the cost of at least doubling the complexity of the decoding mechanism the gain is only doubled. Similarly, various elementary transformations such as differentiation to obtain the mean rate of change will not add to the maximum capacity of the code. This latter alternative probably accounts for some of the qualitative results by earlier workers on pulse spacing but in no way changes the order-of-magnitude difference between the simple code and the detailed-pattern code.

If we wish to investigate the use of detailed-pattern information as a decoding mechanism in a naturally controlled nervous mechanism, then it should first be attempted in a paucicellular system such as the crayfish.[4] Otherwise, with many input fibers to each complex dendritic tree and soma, and with recurrent feedback elements, the synchronization of the many detailed impulse patterns will require an inordinately large and precise system of measurement and a complicated decoding device or process. Thus, one

should look at a favorable invertebrate preparation rather than utilize the mammalian cortex.

The system of the photosensitive cells in the sixth abdominal ganglion of the crayfish also presents many advantages for the experimental approach to this problem, but there are only two receptor cells that can be reliably submitted to the same stimulus and be shown to carry the same information. Indeed, we have seen that cutting one of the fibers did not affect the walking response evoked by the illumination of the ganglion. Furthermore, the activity of the two cells can be recorded simultaneously and separately and the individual pulses can be compared with each other. If the detailed pattern were the code through which the information is transmitted, a high correlation between the two pulse trains at the level of the detailed pattern should be observed.

Instead, we found no correlation (Figs. XV-24 and XV-27d) and occasionally we have seen that only approximately 7 per cent of the pulses show some crosscorrelation dependence (Fig. XV-25a). This must indicate that the detailed timing of the pulses is not a carrier of useful information. These results leave the mean pulse frequency to be considered as the code.

G. Theodoridis, J. Negrete, Guillermina N. Yankelevich, and L. Stark

References

1. J. Negrete, G. N. Yankelevich, G. Theodoridis and L. Stark, Signal information carried by a train of nerve pulses, Quarterly Progress Report No. 74, Research Laboratory of Electronics, M.I.T., July 15, 1964, pp. 255-261.

2. J. Negrete, G. N. Yankelevich, G. Theodoridis and L. Stark, Light inhibitory effects in the crayfish sixth ganglion, Quarterly Progress Report No. 74, Research Laboratory of Electronics, M.I.T., July 15, 1964, pp. 252-254.

3. H. T. Hermann and L. Stark, Random walk response of the crayfish, Quarterly Progress Report No. 61, Research Laboratory of Electronics, M.I.T., April 15, 1961, pp. 230-234.

4. G. P. Moore, Personal Communication, 1964.

5. J. P. Segundo, G. P. Moore, L. J. Stensaas and T. H. Bullock, Sensitivity of neurones in Aplysia to temporal pattern of arriving impulses, J. Exptl. Biol. 40, 643-667 (1963).

6. J. P. Segundo and G. P. Moore, Functional significance of neuronal spike discharge parameters, Bol. Inst. Est. Méd. Biol. 21, 371-373 (1963).

7. G. P. Moore and J. P. Segundo, Stability Patterns in Interneuronal Pacemaker Regulation, Symposium for Biomedical Engineering, San Diego, California, 1963.

8. A. G. Wiersma and R. T. Adams, The influence of nerve impulse sequence on the contraction of different muscles of crustacea, Physiol. Compar. Ecol., Vol. II, pp. 20-33, 1950.

9. S. H. Ripley and A. G. Wiersma, The effect of spaced stimulation of excitatory and inhibitory axons of the crayfish, Physiol. Compar. Ecol., Vol. III, pp. 1-17, 1953.

10. G. F. Poggio and S. J. Viernstein, Time series analysis of impulse sequences of thalmic somatic sensory neurons, J. Neurophysiol. 27, 517-545 (1964).

11. P. D. Wall, J. Y. Lettvin, W. S. McCulloch, and W. H. Pitts, Factors limiting the maximum impulse transmitting ability of an afferent system of nerve fibers, Information Theory, edited by C. Cherry (Academic Press, London, 1956), pp. 329-343.

12. D. M. Mackay and W. S. McCulloch, The limiting information capacity of a neuronal link, Bull. Math. Biophys. 14, 127-135 (1952).

13. C. E. Shannon, Mathematical theory of communication, Bell System Tech. J. 27, 379-423 (1948).

14. L. Stark and H. T. Hermann, The transfer function of a photoreceptor organ, Kybernetik 1, 124-129 (1961).